

Submitted to Astrophysical J.

Sensitivity of r-Process Nucleosynthesis to Light-Element Nuclear Reactions

Taka. Sasaqui^{1,2,6}, T. Kajino^{1,2}

National Astronomical Observatory of Japan

Department of Astronomy, Graduate School of Science, University of Tokyo, 7-3-1 Hongo, Bunkyo-ku, Tokyo 113-0033, Japan

sasaqui@th.nao.ac.jp

G. J. Mathews³, K. Otsuki^{3,5}

Center for Astrophysics, University of Notre Dame, Notre Dame, IN 46556, U.S.A.

and

T. Nakamura⁴

Department of Physics, Tokyo Institute of Technology, 2-12-1 O-Okayama Meguro-ku, Tokyo 152-0033, Japan

ABSTRACT

¹National Astronomical Observatory, 2-21-1 Osawa, Mitaka, Tokyo 181-8588, Japan

²Department of Astronomy, Graduate School of Science, University of Tokyo, 7-3-1 Hongo, Bunkyo-ku, Tokyo 113-0033, Japan

³Center for Astrophysics, Department of Physics, University of Notre Dame, Notre Dame, IN 46556, U.S.A.

⁴Department of Physics, Tokyo Institute of Technology, 2-12-1 O-Okayama Meguro-ku, Tokyo 152-0033, Japan

⁵Department of Astronomy and Astrophysics, LASR103, University of Chicago, 5640 South Ellis Avenue, Chicago, IL 60637

⁶present address : Naka Division, Nanotechnology Products Business Group, Hitachi High-Technologies Corporation, 882, Ichige, Hitachinaka, Ibaraki, 312-0033, Japan

We study the efficiency and sensitivity of r-process nucleosynthesis to 18 light-element nuclear reaction rates. We adopt empirical power-law relations to parameterize the reaction sensitivities. We utilize two different hydrodynamic models for the neutrino-driven winds in order to study the dependence of our result on supernova wind models. We also utilize an exponential model to approximate a wide variety of other plausible conditions for the r-process. We identify several specific nuclear reactions among light neutron-rich nuclei that play a critical role in determining the final r-process nucleosynthesis yields. As an illustration, we examine “semi-waiting” points among the carbon isotopes. We show that not only neutron capture and β -decay, but also (α, n) reactions are important in determining waiting points along the r-process path. Our numerical results from this sensitivity analysis serve foremost to clarify which light nuclear reactions are most influential in determining the final r-process abundances. We also quantify the effects of present nuclear uncertainties on the final r-process abundances. This study thus emphasizes and motivates which future determinations of nuclear reaction rates will most strongly impact our understanding of r-process nucleosynthesis.

Subject headings: r-process nucleosynthesis, nuclear reactions, supernovae

1. Introduction

It is generally believed that the r-process is associated with supernova (SN) explosions (Meyer et al. 1992; Woosley et al. 1994; Witti, Janka & Takahashi 1994), neutron star mergers (Freiburghaus, Rosswog & Thielemann 1999) or gamma-ray bursts (GRB) (Cameron 2001, 2003; Inoue et al. 2003) in which a neutron-rich environment is realized. However, the astronomical site for the r-process has not been unambiguously determined. Clarifying the origin of the r-process and understanding the heavy element production therein are currently important subjects in astrophysics.

In the present work, we attempt to clarify the effects of nuclear physics uncertainties in r-process nucleosynthesis by investigating the dependence of the r-process yields on the nuclear reaction rates and also on the explosion environment. In particular, we first identify the most important light-mass nuclear reactions for the r-process by using the concept of reaction “sensitivity” as defined in Section 2. We discuss the nucleosynthesis network in Section 3, and describe three representative dynamic flow models in Section 4. The results of deduced reaction sensitivities are given in Section 5, where we also investigate the sensitivity of the most important light-element reactions on the explosion conditions. Our defined

“sensitivity” for the efficiency of the nuclear reactions is shown to be a useful measure of the production of actinides. In this context it is also relevant to cosmochronology. In Section 6 an illustration is given based upon a detailed analysis of the waiting point for neutron-rich carbon isotopes. This study highlights both the uncertainty and importance of obtaining experimental data, as well as the role of (α, n) reactions along the r-process path for light nuclei.

1.1. Background

The most probable astronomical site for the r-process is in core-collapse supernovae (e.g. Type II, Ib, Ic SNe). This is supported by the observational fact that the abundance pattern of metal deficient stars has an apparent universality, and is very similar to the solar abundance distribution (Snedden et al. 1996, Honda et al. 2004, etc.). Metal-poor stars ($[\text{Fe}/\text{H}] \leq -3$) have only been influenced by one or two supernovae. The fact that the r-process abundance pattern of these early objects is quite similar to the Solar abundance distribution suggests that supernova explosions have supplied r-process elements in a similar manner both in the past and in more recent times.

Although supernova explosions are not yet fully understood, it has been established (Meyer et al. 1992; Woosley et al. 1994; Wittl, Janka & Takahashi 1994) that some conditions of supernova hydrodynamics (i.e. the hot-bubble region formed by a ν -driven wind) can produce r-process conditions. One such condition is an environment with excess neutrons, i.e. the electron fraction Y_e is less than 0.5. Sufficient neutrons per seed nucleus are a necessary condition for a successful r-process. The r-process occurs effectively when the neutron-to-seed ratio is large. Here, “seed” means nuclei whose mass number is typically between 70 and 120 (including for example ^{78}Ni). Such seed nuclei are made through the α -process (Woosley & Hoffman 1992).

In the wind models the r-process conditions are achieved even for modest Y_e in an environment with high entropy. When the entropy per baryon is large, $s/k_B \geq 200$ (Woosley et al. 1994, Takahashi and Janka 1997), the r-process can occur from the initial condition in which most nuclei are dissociated into alpha particles plus free neutrons and protons. Another condition is that of a short dynamical timescale (Otsuki et al. 2000), where the dynamical time, τ_{dyn} , is defined as the e-fold decay time of the temperature from an initial value of $T_9 = 0.5$ MeV (Qian & Woosley 1996). A short dynamical time can suppress the overproduction of seed nuclei, leaving plenty of free neutrons for the subsequent neutron-capture flow. This is because the temperature drops so rapidly that the α -process becomes ineffective to produce seed. If the dynamical timescale of the neutrino-energized wind is as

short as ~ 5 ms (Otsuki et al. 2000), the 3rd extended r-process peak and even actinide nuclei can be produced.

Moreover, there are now two views about the r-process in supernovae. In one view supernova explosions are the universal site of the r-process (Qian & Woosley 1996). In the other view, not only supernovae but also some other phenomenon has contributed to the r-process (Qian & Wasserburg 2000). Such a site might be the GRB environment (Cameron 2001, 2003; Inoue et al. 2003), hypernovae or collapsars (Pruet, Woosley & Hoffman 2003; Fujimoto et al. 2004), or neutron star mergers (Freiburghaus, Rosswog & Thielemann 1999). In the present work, we will take the former position, *i.e.* that heavy elements, including even the 3rd peak and actinide nuclei, can be sufficiently synthesized in supernovae. In particular, we consider the hot-bubble scenario containing ν -driven winds in gravitational core-collapse Type II supernovae.

Obviously, there remain many questions surrounding the r-process. In order to ultimately identify the astrophysical site for the r-process it is essential to clarify the effects of the uncertainties in the input nuclear physics on the production of r-process nuclei. That is the aim of the present study.

2. Sensitivity Parameter α_i

In analogy with the power-law technique applied by Bahcall (1982) to analyze the sensitivity of nuclear reactions to the Solar neutrino flux, we express the calculated abundances Y_r of r-process nucleosynthesis as

$$\frac{Y_r}{Y_r(0)} = \prod_i \left(\frac{\lambda_i}{\lambda_i(0)} \right)^{\alpha_i(\{\lambda_j\})}, \quad (1)$$

where the subscript r stands for typical r-process elements at the 2nd or 3rd peak, or the actinides. Specifically, we define

$$Y_{2\text{nd}} = \sum_{126 \leq A \leq 134} Y(A), \quad (2)$$

$$Y_{3\text{rd}} = \sum_{191 \leq A \leq 199} Y(A), \quad (3)$$

$$Y_{\text{actinide}} = Y(232), Y(235), \text{ or } Y(238). \quad (4)$$

As usual, $Y(A) = n(A)/\rho N_{AV}$ denotes the number fraction of element A , where $n(A)$ is the number density, ρ is the baryon mass density, and N_{AV} is Avogadro's number. $Y_{2\text{nd}}$,

$Y_{3\text{rd}}$, and Y_{actinide} include the abundances of several typical r-process elements, e.g. $^{129,131}\text{Xe}$ and ^{130}Te for the 2nd peak, $^{194,195,196}\text{Pt}$ for the 3rd peak, and ^{232}Th , ^{235}U , or ^{238}U for the actinides, as shown in Figure 1. Although the r-process abundance peaks change slightly, depending on the adopted hydrodynamics flow models, our conclusions are rather insensitive to the specific peak elements used in Eqs. (2)- (4). The λ_i in Eq. (1) are the thermonuclear reaction rates,

$$\begin{aligned} \lambda_i &\equiv N_{AV} \langle \sigma_i^{(r)}(E) v \rangle \\ &= N_{AV} \left(\frac{8}{\pi \mu_{12} (kT)^3} \right)^{1/2} \int dE \sigma_i^{(r)}(E) E \exp\left(\frac{-E}{kT}\right), \end{aligned} \quad (5)$$

where μ_{12} is the reduced mass of the incident particles, k is Boltzmann’s constant, and T is the temperature of the gas under consideration. $\lambda_i(0)$ is the adopted ”standard” value of the i -th reaction rate in the reaction network as described in Section 3. Thus $Y_r(0)$ ($r = 2\text{nd}$ or 3rd) is the r-process yield for these $\lambda_i(0)$ values. Note, that a variation of the thermonuclear reaction rate from $\lambda_i(0)$ to λ_i must include the corresponding change of the reverse rate.

The reaction cross sections $\sigma_i^{(r)}(E)$ have both resonant and continuum background contributions in general. This can lead to different temperature-dependences of the thermonuclear reaction rates. Nevertheless, most of the reactions of interest here have only a modest temperature dependence. Hence, we here only take into account changes in the strength of λ_i , assuming the same T -dependence. The power index α_i in Eq. (1) is hereafter called the ”sensitivity” parameter.

2.1. Dependence on the Astrophysical Environment

In general, the sensitivity parameters α_i will depend upon the physical conditions of the r-process site. Previous studies (e.g. Meyer et al. 1992; Woosley et al. 1994; Qian and Woosley 1996; Otsuki et al. 2000; Terasawa et al. 2002) have identified four physical parameters which characterize the physical conditions of the r-process. These are: 1) the entropy per baryon s/k ; 2) the expansion time scale τ_{dyn} ; 3) the initial electron fraction $Y_{e,i}$, and the asymptotic boundary temperature T_a of the adopted wind model. Values of these parameters appropriate to the models considered here will be given in the Section 4.

Our adopted sensitivity formula, Eq. (1), has several advantages: First, although r-process nucleosynthesis in SN explosions is complicated, the dependence of the final yields on each nuclear reaction rate is expressed in a simple separable form. This makes the analysis of the reaction sensitivity very simple no matter how complex the explosion dynamics are. Secondly, Eq. (1) represents even the highly non-linear effects of the complicated reaction

processes in large-scale nuclear reaction networks. The larger the $|\alpha_i|$, the more strongly the r-process yields depend on the i-th nuclear reaction rate. If the α_i are close to unity, the r-process yields are linearly dependent on that thermonuclear reaction rate. If the α_i are close to 0, the r-process yields are not affected. Note, however, that $\alpha_i = 0$ does not mean that the r-process is totally independent of the i-th nuclear reaction. For example, $\alpha_i \approx 0$ can occur whenever the reaction collision time scale, $t_{coll} = (n(A)\sigma v)^{-1}$, is smaller than the expansion time scale, i.e. $t_{coll} \ll \tau_{dyn}$, as is the case for a classical r-process.

2.2. Incoherent Approximation

Since α_i is a function of the λ_j 's, the logarithm of Eq. (1) can be written as a Taylor series expansion in powers of $\log(\lambda_i/\lambda_i(0))$

$$\begin{aligned} \log\left(\frac{Y_r}{Y_r(0)}\right) &= \sum_i \alpha_i(\{\lambda_j\}) \log\left(\frac{\lambda_i}{\lambda_i(0)}\right) \\ &= \sum_i \alpha_i(0) \log\left(\frac{\lambda_i}{\lambda_i(0)}\right) \\ &\quad + \frac{1}{2} \sum_{i,j} \left(\frac{\partial \alpha_j(0)}{\partial \log(\lambda_i/\lambda_i(0))} + \frac{\partial \alpha_i(0)}{\partial \log(\lambda_j/\lambda_j(0))} \right) \log\left(\frac{\lambda_i}{\lambda_i(0)}\right) \log\left(\frac{\lambda_j}{\lambda_j(0)}\right) \\ &\quad + \text{higher order terms,} \end{aligned} \tag{6}$$

where $\alpha_i(0) \equiv \alpha_i(\{\lambda_j = \lambda_j(0) \text{ for all } j\})$. The factor $(\partial \alpha_j(0)/\partial \log(\lambda_i/\lambda_i(0)) + \partial \alpha_i(0)/\partial \log(\lambda_j/\lambda_j(0)))$ in the second term does not vanish in general. In practice, however, this coherent term between λ_i and λ_j ($i \neq j$) is small for the adopted standard $\lambda_i(0)$ values. Hence we can set $\lambda_i/\lambda_i(0) \approx 1$ and $\log(\lambda_i/\lambda_i(0)) \ll 1$. Equation (6) is thus well approximated by only the first sum of the power series

$$\log\left(\frac{Y_r}{Y_r(0)}\right) \approx \sum_i \alpha_i(0) \log\left(\frac{\lambda_i}{\lambda_i(0)}\right). \tag{7}$$

The validity of this incoherent approximation will be justified in numerical analysis below in Appendix A.

Although several important reaction cross sections of the light-mass nuclei have been studied both experimentally and theoretically, they still have appreciable uncertainties which may affect the final r-process yield. These will be discussed in Section 3.

The adopted range of $\lambda_i/\lambda_i(0)$ may be beyond the range to be justified in the incoherent approximation (6). Nevertheless, our calculated α_i values for a wide range of $\lambda_i/\lambda_i(0)$ are

still useful as a means to characterize the associated changes in Y_r to be expected as more precise experiments or theoretical determinations of reaction rates become available.

3. Nucleosynthesis Network

For the calculations of r-process nucleosynthesis, we employ the reaction network used in Otsuki et al. (2003), which was developed from the original dynamical network code calculations described in Meyer et al. (1992), Woosley et al. (1994), and Terasawa et al. (2001) so that it includes light neutron-rich nuclei (with $Z \leq 10$). These light neutron-rich nuclei were shown to be important for a successful r-process in models with a short dynamical timescale (Terasawa et al. 2001). They play the significant roles in the production of seed elements in the earlier stage of α -rich freeze-out prior to the r-process (Woosley & Hoffman 1992; Meyer et al. 1992; Woosley et al. 1994). Even so, most reaction rates of extremely neutron-rich radioactive nuclei are still unmeasured or poorly known experimentally. Several other nuclear reaction cross sections at low energies of astrophysical interest have been measured experimentally, however, those are still limited to the reactions of stable and long lived radioactive nuclei (e.g. Angulo et al. 1999). The individual rates of the most important 18 light-element reactions and their adopted uncertainties are listed in Table 1. Several important modifications have been made in the present reaction network.

3.1. $\alpha(\alpha n, \gamma)^9\text{Be}$

The $\alpha(\alpha n, \gamma)^9\text{Be}$ reaction is of particular importance in the neutron-rich r-process models as has been noted by a number of authors (Delano & Cameron 1971; Meyer et al. 1992; Wittl et al. 1994). As such, it has been intensively studied in recent years (Angulo et al. 1999; Utsunomiya et al. 2001; Buchmann et al. 2001; Descouvemont 2002; Mukha et al. 2005). In the lower part of Figure 1 we show three currently used thermonuclear reaction rates for this reaction (Caughlan & Fowler 1988 (CF88); Angulo et al. 1999 (NACRE); Sumiyoshi et al. 2002). In the upper part of this figure we show the calculated r-process abundance yields, based upon these rates, using a wind model given in Otsuki et al. (2003). Although three reaction rates are in reasonable agreement (within factor of three) at relevant temperatures ($0.1 \leq T_9 \leq 10$) for the r-process, the final abundance yields of the actinide elements are very sensitive to their difference even at the 30% level at $1 \leq T_9 \leq 5$ and show appreciable differences. This affects cosmochronology based upon the ratio of long-lived radioactive elements, thorium (Th) and uranium (U), to typical r-process elements such as europium (Eu). In this specific model, for example, the estimated age difference in the Th/Eu-cosmochronometer

(Cowan et al. 1997; Schatz et al. 2002; Otsuki et al. 2003) turns out to be $\Delta T = 9.35$ Gy when we apply the calculated abundances for the CF88 and Woosley & Hoffman (1992) rates, while it is only $\Delta T = 3.00$ Gy for the NACRE and Sumiyoshi et al. (2002) rates.

In the present paper we take the three-body reaction rate for $\alpha(\alpha n, \gamma)^9\text{Be}$ from the network estimate (Sumiyoshi et al. 2002) based on the experimental data of Utsunomiya et al. (2001), which spans the low energy region of astrophysical interest. Since direct measurement of the radiative three-body capture reaction $\alpha(\alpha n, \gamma)^9\text{Be}$ is impossible, Utsunomiya et al. (2001) measured photodisintegration cross section of ^9Be with quasi-monochromatic γ rays produced by means of inverse Compton scattering of laser photons. Applying the principle of the detailed balance to the measured cross section, they obtained the forward reaction cross section.

Although the data include all relevant resonance states of astrophysical interest, there is still $\pm 35\%(1\sigma)$ uncertainty in the thermonuclear reaction rates among those of Utsunomiya et al. (2001), Angulo et al. (1999), Mukha et al. (2005), and Buchmann et al. (2001). This arises from different estimates of resonance parameters from (γ, n) , (e, e') , and β -decay experiments as discussed in details by Sumiyoshi et al. (2002).

3.2. $\alpha(t, \gamma)^7\text{Li}$

We take the reaction rate for $\alpha(t, \gamma)^7\text{Li}$ from Kajino (1986) and Kajino, Toki, and Austin (1987) as recommended by Angulo et al. (1999). This reaction has been studied very well by several experimental groups (Brune et al. 1994, and references therein) for the importance in the Big-Bang nucleosynthesis along with the mirror conjugate $\alpha(^3\text{He}, \gamma)^7\text{Be}$ reaction for solving the missing solar neutrino problem (Adelberger et al. 1998). The NACRE compilation, which shows $\pm 10\%(1\sigma)$ uncertainty of the $\alpha(t, \gamma)^7\text{Li}$ rate, has recently been reevaluated theoretically by Descouvemont et al. (2004) (hereafter ADNDT04) using the R-matrix analysis.

Although the new ADNDT04 analysis shows even smaller uncertainty of $\pm 4\%(1\sigma)$ than the NACRE compilation, more general treatment of the error bar estimate (Smith et al. 1993) indicates $\pm 20\%(1\sigma)$ uncertainty. A recent Monte Carlo analysis (Nollett & Burles 2000) has indicated even larger uncertainty of $\pm 30\%(1\sigma)$ at lower temperature $T_9 = 0.1 - 0.2$. In view of this, we adopt $\pm 30\%(1\sigma)$ uncertainty in the present paper.

3.3. ${}^7\text{Li}(n,\gamma){}^8\text{Li}$

We take the reaction rate for ${}^7\text{Li}(n,\gamma){}^8\text{Li}$ from Nagai et al. (1991b). Their measured cross section at the neutron energy of 30keV, $\sigma(30\text{keV}) = 39.3 \pm 6.0 \mu\text{b}$, is consistent with the thermal reaction cross section tabulated by Mughabghab et al. (1981), $\sigma_{th} = 0.045 \pm 0.003\text{b}$, when one expects $1/v$ extrapolation from the thermal neutron energy to 30keV. However, Nagai’s measurement is systematically larger by 30% - 50% than those measured by Wiescher et al. (1989) in the energy range 25-420keV. We therefore estimate that the uncertainty of $\pm 35\%(1\sigma)$ still remains for the ${}^7\text{Li}(n,\gamma){}^8\text{Li}$ reaction rate at astrophysical energies.

3.4. ${}^8\text{Li}(\alpha,n){}^{11}\text{B}$

The reaction rate for ${}^8\text{Li}(\alpha,n){}^{11}\text{B}$ is taken from Gu et al. (1995). This reaction was identified to be a critical nuclear reaction of producing the intermediate-to-heavy mass elements in some inhomogeneous Big-Bang nucleosynthesis models (Malaney & Fowler 1988, Boyd & Kajino 1989, Kajino & Boyd 1990) as well as for r-process nucleosynthesis (Terasawa et al. 2001, Kajino, Wanajo & Mathews 2002). Ishiyama et al. (2004) have recently carried out very precise measurements of the exclusive reaction cross section for ${}^8\text{Li}(\alpha,n){}^{11}\text{B}^*$ as well as for ${}^8\text{Li}(\alpha,n){}^{11}\text{B}_{gs}$. Their result confirms that the transitions leading to several excited states of ${}^{11}\text{B}$ make a predominant contribution to the total reaction cross section, which is in good agreement with the previous measurements of the inclusive reaction cross section (Boyd et al. 1992; Gu et al. 1995; Mizoi et al. 2000; Paradellis et al. 1990).

Although each experiment reported $\pm 20\%$ (Gu et al. 1995), $\pm 60\%$ (Mizoi et al. 2000), or $\pm 30\%$ (Ishiyama et al. 2004) uncertainty of the measured cross section at $0.6\text{MeV} \leq E$, their absolute values are very different from one another by factor 1.7 - 2.1. We are therefore forced to estimate a factor of two uncertainty for the ${}^8\text{Li}(\alpha,n){}^{11}\text{B}$ reaction rate at astrophysically relevant energies $E \leq 0.5\text{MeV}$.

3.5. ${}^9\text{Be}(n,\gamma){}^{10}\text{Be}$ and ${}^A\text{B}(n,\gamma){}^{A+1}\text{B}$ (A=11-14)

The reaction rate for ${}^9\text{Be}(n,\gamma){}^{10}\text{Be}$, ${}^{11}\text{B}(n,\gamma){}^{12}\text{B}$, ${}^{12}\text{B}(n,\gamma){}^{13}\text{B}$, and ${}^{13}\text{B}(n,\gamma){}^{14}\text{B}$ are taken from Rauscher et al.(1994). Although these rates were calculated by using the best available resonance parameters, there are still many uncertainties which arise from assumed neutron spectroscopic factors, γ -widths, etc. It therefore is a fair estimate that these reaction rates have at least a factor of two uncertainty.

There is no datum available for the $^{14}\text{B}(n,\gamma)^{15}\text{B}$ reaction rate. It is expected, however, that the radiative neutron-capture from scattering s- and p-waves occurs in a similar manner to the $^{13}\text{B}(n,\gamma)^{14}\text{B}$ reaction at low energies of astrophysical interest because of their similar spin-angular momentum coupling scheme. We therefore estimate the reaction rate for $^{14}\text{B}(n,\gamma)^{15}\text{B}$ from the $^{13}\text{B}(n,\gamma)^{14}\text{B}$ rate given by Rauscher et al. (1994), with the correction due to different reaction Q values being taken into consideration.

3.6. $^A\text{C}(n,\gamma)^{A+1}\text{C}$ (A=12-19) and $^{18}\text{C}(\alpha,n)^{21}\text{O}$

The reaction rate for $^{12}\text{C}(n,\gamma)^{13}\text{C}$ is taken from Nagai et al. (1991a). Gibbons et al. (1961) old uncertain datum, $\sigma(30\text{keV}) = 200 \pm 400\mu\text{b}$, was revised by precise experimental values of Nagai et al. (1991a), $\langle\sigma\rangle = 16.8 \pm 2.1\mu\text{b}$, and Ohsaki et al. (1994), $\langle\sigma\rangle = 15.4 \pm 1.0\mu\text{b}$, which are in reasonable agreement with each other within their 1σ error bars, where $\langle\sigma\rangle$ is the Maxwellian-averaged neutron-capture cross section at the temperature $kT = 30\text{keV}$. They also decomposed direct p-wave and d-wave contributions to the non-resonant neutron capture cross sections (Kikuchi et al. 1998). These new data are also consistent with the measured upper limit of Macklin (1990), $\langle\sigma\rangle < 14\mu\text{b}$. Careful analysis of the combined precise data of Nagai et al. (1991a) and Ohsaki et al. (1994), so as to minimize the reduced- χ^2 by taking account of its error from the χ^2 distribution, indicates $\pm 10\%(1\sigma)$ uncertainty of the $^{12}\text{C}(n,\gamma)^{13}\text{C}$ reaction rate.

Raman et al. (1990) measured the γ -width of the 2^+ state of ^{14}C which lies at 142 keV above the $^{13}\text{C} + n$ particle threshold. Rauscher et al. (1994) assumed predominance of this resonance contribution to the $^{13}\text{C}(n,\gamma)^{14}\text{C}$ cross section. Since the measured γ -width has +40% and -16% error bars (Raman et al. 1990) and the other resonances or direct capture component may contribute to the total reaction rate, we estimate a factor of two uncertainty of the reaction rate for $^{13}\text{C}(n,\gamma)^{14}\text{C}$.

The $^{14}\text{C}(n,\gamma)^{15}\text{C}$ cross section at astrophysical low energies was measured by Beer et al. (1992) in direct neutron-capture experiments, and also by Howath et al. (2002) and Nakamura et al. (2003) via Coulomb dissociation of ^{15}C . These authors report respectively $\pm 25\%$, $\pm 35\%$, and $\pm 10\%$ uncertainties of their Maxwellian-averaged neutron-capture cross sections at the temperature $kT = 23\text{keV}$. For its importance in inhomogeneous Big-Bang nucleosynthesis of intermediate-to-heavy mass nuclei (Wiescher, Gorres & Thielemann 1990; Kajino, Mathews & Fuller 1990), another Coulomb dissociation experiment (Pramanik et al. 2003) was carried out. The result is more consistent with the direct neutron-capture experiment. Absolute values of these four reaction rates unfortunately differ by a factor of 2-4 from one another. Therefore we estimate a factor of four uncertainty of the reaction rate

for $^{14}\text{C}(n,\gamma)^{15}\text{C}$.

The reaction rates for $^{15}\text{C}(n,\gamma)^{16}\text{C}$ and $^{16}\text{C}(n,\gamma)^{17}\text{C}$ are taken from Rauscher et al. (1994). These rates have at least a factor of two uncertainty for the same reasons discussed above for the $^9\text{Be}(n,\gamma)^{10}\text{Be}$ and $^A\text{B}(n,\gamma)^{A+1}\text{B}$ ($A = 11, 12, \text{ and } 13$) reactions.

For the other neutron-rich carbon isotopes we make use of Hauser-Feshbach (HF) estimates for the (n,γ) and (α,n) rates, as has been done in previous studies (e.g. Terasawa et al. 2001). We utilize these estimates even though it is generally believed that the HF model is a poor approximation for light nuclei (as well as for exotic neutron rich nuclei) due to the low density of states for these nuclei. Nevertheless, HF estimates are easy to obtain and are often within a factor of two (Mathews et al 1983) of the true cross sections. Direct capture cross sections would provide a lower limit to the cross sections (Mathews et al. 1983) if the relevant spectroscopic factors were known. However, such nuclear data for most of the neutron-rich nuclei of interest here have yet to be obtained. As such, we consider simple HF estimates as good as can be obtained at the present time. They are consistent with other network applications in the field, and provide an adequate basis on which to judge which cross sections have the most sensitivity for r-process nucleosynthesis. We note that only the reaction rate for $^{18}\text{C}(n,\gamma)^{19}\text{C}$ is estimated from the measured cross section using the Coulomb dissociation method by Nakamura et al.(1999).

Extensive neutron-rich nuclei and their associated nuclear reactions were also added (Nakamura et al. 1994; Fukuda et al. 2004; Otsuki et al. 2003, Terasawa et al. 2001, 2002) so that the updated network applies to many different kinds of wind models. Wanajo et al. (2002) suggested that the low-mass neutron-rich nuclei would be less important in their specific models than that found by Terasawa et al. (2001) for a low adopted asymptotic temperature. As we will discuss in the next sections, however, these nuclei play an important role in any wind models. We finally note that we calculate the nucleosynthesis sequence from the NSE, α -process, α -rich freeze-out, r-process and subsequent beta-decay and alpha-decay in a single network code rather than to split the calculation into two parts as was done in Woosley et al. (1994). These modifications are important for our studies of the nuclear reaction sensitivity of r-process nucleosynthesis.

4. Neutrino-Driven Wind Models

Our purpose is to clarify the dependence of r-process nucleosynthesis on individual nuclear reaction rates. The sensitivity parameters α_i , however, depend on thermodynamic quantities specific to the explosion conditions. Possible astrophysical sites for the r-process

include Type II SNe, neutron-star mergers, and several others (e.g. Mathews and Cowan 1990). The detailed explosion dynamics for these sites, however, are not yet quantitatively known.

Even in the presently popular paradigm of neutrino-driven winds from Type II SNe, the physical conditions of the r-process are dependent on details of the adopted numerical simulation (Meyer et al. 1992; Woosley et al. 1994; Wittl et al. 1994; Takahashi et al. 1994; Qian & Woosley 1996; Cardall & Fuller 1997; Hoffman et al. 1997; Otsuki et al. 2000, 2003; Sumiyoshi 2000; Thompson, Burrows & Meyer 2001; Wanajo et al. 2001). In this article, therefore, we adopt three different schematic parameterizations of the r-process conditions. One is a fast steady-state neutrino-driven wind (Otsuki et al. 2000); the other is a slow hydrodynamic wind (Woosley et al. 1994; Qian & Woosley 1996). The third is an exponential model as used in Otsuki et al. (2003).

4.1. Fast Steady-State Wind Model

One model we consider is that of a fast spherical steady-state flow model for the neutrino-driven wind (Qian & Woosley 1996; Takahashi & Janka 1997; Otsuki et al. 2000, 2003; Thompson et al. 2001; Wanajo et al. 2001). Otsuki et al. (2000) and Sumiyoshi et al. (2000) found that the r-process can occur in such neutrino-driven winds even for moderate entropies ($s/k \approx 100\text{-}300$) as long as the dynamical expansion timescale becomes much shorter than the collision timescale of neutrino-nucleus interactions. We note that there has been some discussion (e.g. Thompson et al. 2001) of a very fast r-process with high $Y_e \geq 0.485$. In such an extreme alpha-rich environment it is possible that the 3α reaction competes with the $\alpha(\alpha, n)^9\text{Be}$ reaction to assemble heavy nuclei. In this case the r-process yields might also have some sensitivity to the 3α reaction. However, we do not investigate that possibility here.

For the present application, such hydrodynamic flow can be approximated (Otsuki et al. 2003) by solving the following non-relativistic equations:

$$4\pi r^2 \rho v = \dot{M} , \tag{8}$$

$$\frac{1}{2}v^2 - \frac{GM}{r} + N_{AV} s_{rad} kT = E , \tag{9}$$

$$s_{rad} = \frac{11\pi^2}{45\rho N_{AV}} \left(\frac{kT}{\hbar c} \right)^3 , \tag{10}$$

where \dot{M} is the rate at which matter is ejected by neutrino heating from the surface of the proto-neutron star.

The total energy E in Eq. (9) is fixed by a boundary condition on the asymptotic temperature T_a

$$E = N_{AV} s_{rad} k T_a . \quad (11)$$

We only take into account photons and e^\pm pairs for relativistic particles in the estimate of the entropy, s_{rad} , in Eq. (11). For simplicity, we utilize an adiabatic, constant-entropy wind rather than to compute the neutrino heating explicitly (Otsuki et al. 2000, Wanajo et al. 2001). We assume a constant neutrino luminosity of $L_\nu = 10^{51} \text{ergs s}^{-1}$ for each neutrino species.

This model has four parameters. They are the neutron-star mass, entropy, boundary temperature, and mass-loss rate. We here adopt one typical flow which characterizes the “fast wind” with a short dynamical explosion timescale, $\tau_{dyn} = 5 \text{ ms}$, and moderately high entropy per baryon, $s/k = 300$. Parameters for this model are summarized in Table 2. As shown in Otsuki et al. (2003), this parameter set well reproduces the universal abundance pattern of neutron-capture elements.

4.2. Slow Wind Model

A dynamical Type II SN explosion and the subsequent r-process in the neutrino-driven wind above the proto-neutron star were calculated by Woosley et al. (1994). Their numerical results were based upon the spherically symmetric hydrodynamic code described in Wilson & Mayle (1993). That calculation included a number of refinements over previous treatments of the hydrodynamics and convection so that the evolution could be followed to more than 10 s after the core bounce. Such late times are necessary to describe properly the mass-loss rate and neutrino excess in the wind. Although this numerical simulation demonstrated for the first time that the r-process could occur in delayed neutrino-heated SNe, several difficulties were subsequently identified. First, independent non-relativistic numerical models (e.g. Wittl et al. 1994, Takahashi et al. 1994) had difficulty producing the required entropy $s/k \sim 400$ as indicated by Woosley et al. (1994). Second, even should the entropy be high enough, the effects of neutrino absorption $\nu_e + n \rightarrow p + e^-$ and $\nu_e + A(Z, N) \rightarrow A(Z + 1, N - 1) + e^-$ decrease the neutron fraction and prohibit the r-process (Meyer 1995). Otsuki et al. (2000) showed that this is generally the case when the expansion of the neutrino-driven wind is slow.

Nevertheless, this “slow wind” model of Woosley et al. (1994) is still attractive, as a source for the 1st and 2nd r-process peaks. We therefore adopt the flow model of trajectory 40 in Woosley et al. (1994) as a typical “slow wind” model with high entropy $s/k \sim 400$

and a large dynamical expansion timescale $\tau_{dyn} \approx 300$ ms. The characteristic parameters of this wind model are compared with those of the “fast wind” model in Table 2.

4.3. Exponential Model

We also utilize an exponential model similar to that employed by Meyer and Brown (1997) in order to roughly approximate conditions for the r-process which might occur in lower-entropy, low Y_e environments such as prompt SNe (Hillebrandt et al. 1984, Sumiyoshi et al. 2001, Wanajo et al. 2003) or neutron-star mergers (Freiburghaus, Rosswog, & Thielemann 1999).

Under the condition that

$$s = \frac{11\pi^2}{45\rho N_{AV}} \left(\frac{kT}{\hbar c} \right)^3 = \text{const.} \quad , \quad (12)$$

the temperature and matter density are given by

$$T_9(t) = T_9(0) \exp(-t/\tau_{dyn}) + T_a, \quad (13)$$

$$\rho(t) = \rho(0)(T_0/T)^3 \quad (14)$$

$$\rho(0) = 3.3 \times 10^8 \text{ gcm}^{-3}, \quad (15)$$

where $T_9(0) = 8.40$, and T_a is the asymptotic temperature (Terasawa et al. 2002, Otsuki et al. 2003) of the wind as given in Eq. (11). This temperature determines the freeze-out of neutron-capture flow. Given the adiabatic entropy per baryon s/k , the matter density evolves so that it satisfies Eq. (11) where one replaces s_{rad} by s . In a more realistic calculation with fixed entropy there will be an increase in temperature at the end of the expansion as electron pairs annihilate (e.g. Woosley et al. 1994). However, given the schematic nature of the exponential model employed here, we ignore that effect on the temperature evolution.

The parameter sets we use in the exponential models are summarized in Tables 3- 6. Because sensitivities can only be meaningfully compared between models in which a similar abundance pattern is produced, we have selected parameter sets which lead to nearly the same final abundance pattern, as displayed in Figure 1, while simultaneously varying two parameters. The three models with fixed Y_e and T_a in Table 3 thus give the dependence of the sensitivity on a simultaneous variation of the dynamical timescale τ_{dyn} and entropy s/k . Similarly, Tables 4 and 5 with fixed τ_{dyn} and T_a show effects of a simultaneous variation of s/k and Y_e . Note that we fix τ_{dyn} at a different value in Table 4 ($\tau_{dyn} = 1.0$ ms) and Table 5 ($\tau_{dyn} = 5.0$ ms) in order to avoid almost degenerate choice of the two parameters s/k and Y_e . Table 6 with fixed τ_{dyn} and Y_e then involves a simultaneous variation of s/k and T_a .

It is important to consider such a wide variety of models. For example, neutron star mergers (Freiburghaus, Rosswog & Thielemann 1999) have a low $Y_e \leq 0.2$, while Y_e typically ranges from 0.42 to 0.47 in the ν -driven winds of core-collapse supernovae (Woosley et al. 1994). Although such merger models involve even lower entropy and Y_e than the models considered here, these parameter sets, nevertheless, provide some indication as to the dependence of the r-process sensitivities as Y_e is decreased.

5. Results

5.1. Most Important Light Nuclear Reactions

In network calculations, the abundance evolution can be written as

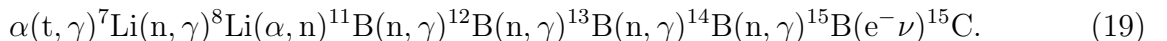
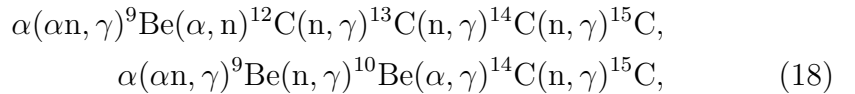
$$\frac{dY_i}{dt} = - \sum_{j \cdots k} \lambda_{ij \cdots k}^{lm \cdots n} Y_i Y_j \cdots Y_k + \sum_{lm \cdots n} \lambda_{lm \cdots n}^{ij \cdots k} Y_l Y_m \cdots Y_n \quad , \quad (16)$$

where Y_i is the number abundance, and $\lambda_{ij \cdots k}^{lm \cdots n}$ and $\lambda_{lm \cdots n}^{ij \cdots k}$ are the destruction ($i + j + \cdots + k \rightarrow l + m + \cdots + n$) and production ($i + j + \cdots + k \leftarrow l + m + \cdots + n$) of the i -th nucleus, respectively. To identify which reactions are most important in the r-process we define the flux at a particular nucleus, j , as

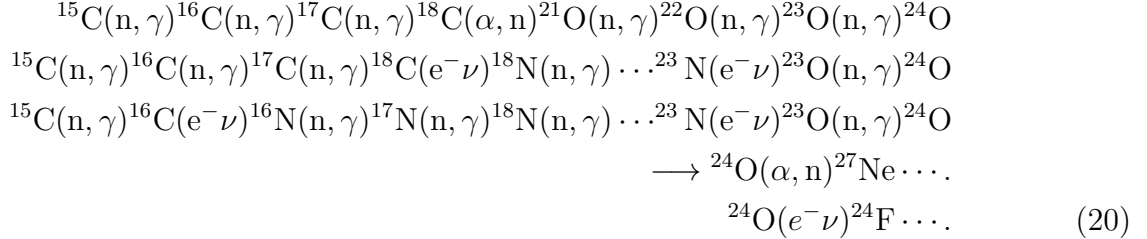
$$F_{ij}(t) = \int_0^t \left[\frac{dY_i}{dt'}(i \rightarrow j) - \frac{dY_j}{dt'}(j \rightarrow i) \right] dt' \quad . \quad (17)$$

The $F_{ij}(t)$ is the net nuclear flux through the nucleus j from $t = 0$ to a time t . By setting $t \geq t_f$, where t_f is the freezeout time of the r-process, we can quantitatively determine which nuclear reaction experiences the largest flux throughout the nucleosynthesis. We define t_α and t_n at which the temperature of the expanding wind becomes $T_\alpha = 0.5 \text{ MeV}$ and $T_n = T_\alpha e^{-1}$, respectively. T_α is the typical temperature at the beginning of the α -process when the system drops out of the nuclear statistical equilibrium (NSE), and T_n is the temperature near the end of the α -process. We can define the expansion time scale τ_{dyn} in Eq. (13) as a typical duration time for the α -process nucleosynthesis, i.e. $\tau_{dyn} = t_n - t_\alpha$. After t_n , successive neutron-capture flow on intermediate-to-heavy mass unstable nuclei is established.

In this way we have found three equally important main-flow paths among the light-mass nuclei. These paths predominate in all of the models considered here. They are,



This is consistent with the results of Terasawa et al. (2001). We have also identified the main flow-paths to nuclei beyond ^{15}C ,



The first nuclear reaction chain through ^9Be and ^{12}C in Eq. (17) is well studied in the literature (Woosley & Hoffman 1992, Woosley et al.1994; Wittl et al. 1994; Otsuki et al. 2000; Terasawa et al. 2001). It plays an important role in the α -process. The second nuclear reaction chain through ^{10}Be in Eq. (17) and the chain of Eq. (18) are the newly identified main flow paths along with the extended flow of Eq. (19). The significance of the flows identified in Eqs. (18) and (19) is universal and will be further discussed below.

5.2. Reaction Sensitivity in Fast and Slow Wind Models

We carried out network calculations and obtained the final abundances of r-process elements. The 18 most relevant reactions in Table 1 were analyzed to derive the sensitivity parameters as formulated in Section 2. These results are summarized in Tables 7 and 8. Shown in the last two columns are the current importance of each reaction at $\pm 2\sigma$ uncertainties in the r-process nucleosynthesis, which is defined by

$$\frac{Y_r}{Y_r(0)} \equiv \frac{Y_r(0) + \delta Y_r}{Y_r(0)} \approx \left(1 + \frac{\delta \lambda_i}{\lambda_i(0)}\right)^{\alpha_i}, \tag{21}$$

where we set $\delta \lambda_i = \pm 2\sigma_i \lambda_i(0)$ with σ_i tabulated in Table 1. We here take the average of ^{235}U and ^{238}U as typical of r-process yields. These can be used to infer which reactions most strongly affect the abundance pattern of heavy r-process elements.

5.2.1. Fast-flow models

We first discuss the results for the fast flow model (Sect. 4.1). We show in Fig. 2 an example of how to determine the sensitivity parameter α_i for the $\alpha(\alpha\text{n}, \gamma)^9\text{Be}$ reaction. The top left, top right, lower left, and lower right panels show the abundance ratios for the 2nd

peak, 3rd peak, Th, and U elements, respectively, as defined by Eqs.(1) - (4). Shaded regions indicate the $\pm 1\sigma$ uncertainties in the reaction rate for $\alpha(\alpha n, \gamma)^9\text{Be}$, as given in Table 1, and $\log(\lambda_i/\lambda_i(0)) \equiv \log([\lambda_i(0) + \delta\lambda_i]/\lambda_i(0))$. The sensitivity parameter α_i is the logarithmic derivative of $Y_r/Y_r(0)$ at $\lambda_i/\lambda_i(0) = 1$, thus the variation of $\log(Y_r/Y_r(0))$ in the shaded region is linearly approximated by Eq.(7) very well once we calculate $\alpha_i \approx \alpha_i(0)$.

The abundance for the 2nd peak (in the top left panel) has a maximum value at $\log \lambda_1/\lambda_1(0) = 0.35$, while the abundance for the 3rd peak (in the top right panel) is a monotonically decreasing function of $\lambda_1/\lambda_1(0)$. Increasing λ_1 makes the α -capture process more important. This leads to an increase in the abundance of seed nuclei, which are mainly produced by the α -process, and a decrease in the abundance of free neutrons at the end of the α -process. This decrease in the neutron-to-seed ratio is not favorable for the r-process. It is the reason that the abundances of both the 2nd and 3rd peak elements decrease for $\log(\lambda_1/\lambda_1(0)) \geq 0.35$. On the other hand, only the abundance for the 2nd peak decreases toward smaller $\lambda_1/\lambda_1(0)$ in the region of $\log(\lambda_1/\lambda_1(0)) \leq 0.35$. Decreasing λ_1 means that the α -process becomes inefficient. This results in a decrease in the abundance of seed nuclei, increasing the neutron-to-seed ratio.

Reactions (2) and (4), i.e. $\alpha(t, \gamma)^7\text{Li}$ and $^8\text{Li}(\alpha, n)^{11}\text{B}$, exhibit a similar trend to that of the $\alpha(\alpha n, \gamma)^9\text{Be}$ reaction. The reason for this is the same as for that reaction. The neutron-capture reactions (3), (5), (7), (9), (11), (13) and (15) show similar results to one another as expected from the calculated sensitivity parameters in Table 7. As λ_i for these rates increases, the abundances of the 2nd peak increase while the 3rd peak decreases. As λ_i increases, these neutron-capture processes more efficient. Neutrons are therefore exhausted at an earlier stage and heavier elements do not form. Thus, the abundances of the 3rd peak decrease. On the other hand, abundances of the 2nd peak increase with λ_i because nuclei capture neutrons efficiently up to the N=82 closed shell.

The r-process has almost no sensitivity to the n-capture reactions (8), (10), (12), (14), (16) and (17). Therefore, variation of these reactions within our adopted uncertainties has almost no effect on the r-process abundances. On these reaction paths, there are no important reactions other than neutron-capture.

5.2.2. *Slow-flow models*

The sensitivity to charged-particle reactions is relatively higher than the neutron-capture reactions in the slow flow model (Sect.4.2) as indicated in Table 8. As described above, the α -process is very sensitive to the temperature. In the slow model, the α -capture process

lasts for a longer time than the fast flow model. This is because the temperature is kept high enough for nuclei to overcome the Coulomb barrier. Therefore, in the slow models, the reaction flow passes close to the β stability line.

Comparing the results of the two flow models, we find that the sensitivities are very dependent on the expansion timescale.

5.3. Sensitivity in Exponential Models

In this subsection we discuss the dependence of the reaction sensitivities on a wide range of dynamical conditions for the r-process based upon the exponential model described in Sect. 4.3.

Figures 3 - 6 illustrate the dependence of the sensitivities of the three most important reactions (1)-(3) on various characteristic quantities based upon the parameter sets shown in Tables 3 - 6. In extreme conditions which have a wide range of τ_{dyn} and even very low Y_e such as in the prompt SN explosions or neutron-star mergers, we need to know the reaction sensitivities for more nuclear reactions in Table 1. We therefore summarize in Tables 9 - 13 the detailed sensitivity results of the extended reactions (1)-(6) and (15) for each model. From these results we deduce that the dynamical timescale τ_{dyn} and asymptotic temperature T_a can significantly affect the sensitivity, while s/k and Y_e do so only moderately. Note the difference of vertical scale for α_i in Figure 4 ($\tau_{dyn} = 1.0$ ms) and Figure 5 ($\tau_{dyn} = 5.0$ ms). Although the sensitivity does not strongly change for various s/k or Y_e , absolute α_i values are generally larger for shorter dynamical timescale.

These indicate that knowing τ_{dyn} for the true r-process environment is most crucial for determining the reaction sensitivities. Indeed, τ_{dyn} determines whether the α -process dominates the neutron-capture process, and is thus the key parameter to understanding the r-process in supernova heated winds. The second most important parameter is T_a . This parameter determines how long the neutron-capture flow endures before freezeout.

However, τ_{dyn} and T_a can only be estimated from a realistic, definitive model for SN explosions which does not yet exist. Moreover, actinide elements are the most sensitive to all astrophysical environmental parameters (Otsuki et al. 2003; Sasaqui, Kajino & Balantekin 2005), as clearly shown in Figures 3 - 6 and Tables 9 - 13, because a slight variation of the nuclear reaction rate results in a large effect on the yield, as shown in Fig 1. This makes determining of accurate light-element reaction rates crucial for cosmochemistry.

6. Detailed Analysis of the Nuclear Reaction Flow

6.1. Carbon Isotopes; Neutron-capture vs. α -capture

We found in Sect.5 that many carbon isotopes are on the most important nuclear reaction chains. We therefore study the importance of these nuclei in the r-process nucleosynthesis more in detail in this section. There are four important flow paths: They are the neutron-capture, the photo-disintegration, the α -capture and the β -decay reactions (Figure 7).

The time evolution of the abundances is given,

$$\begin{aligned}
 \frac{dY_{iC}}{dt} = & -N_A \langle \sigma v_{iC(n,\gamma)} \rangle \rho Y_{iC} Y_n + \lambda_{i+1} Y_{i+1C} \\
 & - \lambda_i Y_{iC} + N_A \langle \sigma v_{i-1C(n,\gamma)} \rangle \rho Y_{i-1C} Y_n \\
 & - N_A \langle \sigma v_{iC(\alpha,n)} \rangle \rho Y_{iC} Y_\alpha + N_A \langle \sigma v_{i+3O(n,\alpha)} \rangle \rho Y_{i+3O} Y_n \\
 & - N_A \langle \sigma v_{iC(\alpha,p)} \rangle \rho Y_{iC} Y_\alpha + N_A \langle \sigma v_{i+3N(p,\alpha)} \rangle \rho Y_p \\
 & - \lambda_\beta Y_{iC} \quad ,
 \end{aligned} \tag{22}$$

where Y_{iC} is the number abundance of a C isotope with mass number i , while Y_{i+1C} , Y_{i-1C} , Y_{i+3N} and Y_{i+3O} represent the nuclei made by (n, γ) , (γ, n) , (α, p) and (α, n) reactions, respectively, and λ_i is the photo-neutron emission rate for ${}^iC(\gamma, n){}^{i-1}C$ which should satisfy the principle of the detailed balance with the forward (n, γ) rate. The most important paths are (α, n) , (n, γ) , and β -decay reactions, as shown by thick solid arrows in Figure 7.

If the neutron separation energy of ${}^{i+1}C$ is large, the (n, γ) capture of iC into the isotope ${}^{i+1}C$ exceeds its (γ, n) photodisintegration. This is the case for ${}^{18}C$, and we show in Figure 8 the net nuclear flux $F_{ij}(t)$ which is defined by Eq.(16). This results in an accumulated abundance of carbon nuclei with the highest neutron separation energies (e.g. ${}^{16}C$ and ${}^{18}C$ in Table 14). It is the reason for the large sensitivity of the r-process to the ${}^{15}C(n, \gamma){}^{16}C$ and ${}^{17}C(n, \gamma){}^{18}C$ reactions (see Table 7).

On the other hand, the α -captures occur until just before the time t_n at which the α -process freezes out and the neutron-capture process effectively starts. The (α, n) reaction in particular, can be as important as the (n, γ) or the inverse reactions (for example, see Figure 8 for ${}^{18}C$). We will describe the ${}^{18}C$ in detail in Section 6.2. In general, β -decay is not important for the abundance evolution of long lived ($t_{1/2} > 1s$) C isotopes (Table 14). The main reactions for C isotopes are (n, γ) and (γ, n) , while the β -decay and α -capture on ${}^{18}C$ operate as an escape route to heavier elements.

These trends also appear in the evolution of other carbon nuclei. For example, the

reaction flux between ^{14}C and ^{15}C , ^{16}C and ^{17}C , and ^{18}C and ^{19}C is similar. Just after t_n , photo-disintegration dominates at ^{15}C , ^{17}C and ^{19}C , because of their small neutron separation energies S_n (see Table 14). However, as the temperature drops the neutron-captures proceed efficiently with no α -captures. The direction of the flux is thus toward heavier nuclei. On the other hand, between ^{15}C and ^{16}C , or between ^{17}C and ^{18}C , the net flux is always toward heavy isotopes by neutron-capture.

6.2. $^{18}\text{C}(n,\gamma)^{19}\text{C}$ and the ^{18}C Waiting Point

A discussion of the $^{18}\text{C}(n,\gamma)^{19}\text{C}$ reaction rate is illuminating as an example of the importance of examining the reaction flow when determining which reactions are most crucial to measure. It also illustrates the uncertainties in the nuclear reaction rates in this region. As noted above, most reaction rates for these light nuclei have not been measured. A measurement of the cross section for the $^{18}\text{C}(n,\gamma)^{19}\text{C}$ reaction (16) in Table 1 was, however, carried out by Nakamura et al. (1999) by using the Coulomb dissociation method of ^{19}C . Applying the principle of the detailed balance to the (γ,n) photodistribution and the (n,γ) neutron-capture, we can obtain the forward (n,γ) cross section shown in Figure 9. This Figure 9 compares cross sections from the HF model and the experiment. The experimental data are about two orders of magnitude larger than the theoretical HF estimates. The experiment by Nakamura et al.(1999) also shows that the neutron separation energy of ^{19}C is 0.530 MeV which is larger than the theoretical estimate of 0.191 MeV. These two measurements lead to a drastic increase of the abundance of ^{19}C (thick solid line in Figure 10) relative to that based upon the HF cross sections (thin solid line in Figure 10).

On the other hand, even with this drastic change in the reaction rate, there is no sensitivity of the r-process to this reaction *i.e.* $\alpha_i \approx 0$. (See Table 7.) The abundance of ^{18}C remains almost unchanged (see Figure 10). In other words, the nuclear flow through ^{18}C is the same regardless of the (n,γ) cross section. This is explained by the fact that the (γ,n) rate is faster than the (n,γ) . The neutron separation energy between ^{18}C and ^{19}C is “small” compared with other carbon nuclei even though it was increased from 0.191 MeV to 0.53 MeV. (See Table 14). Hence, ^{19}C is quickly photo-disintegrated. The reaction path then flows out into heavy elements through $^{18}\text{C}(\alpha,n)^{21}\text{O}$ and even though the (n,γ) rate indirectly affects the r-process, there is essentially no sensitivity of the r-process to this reaction.

It is also of interest that the reaction flow stalls for an instant at ^{18}C . The competition between (α,n) and β -decay is then important. An experimental measurement of the $^{18}\text{C}(\alpha,n)^{21}\text{O}$ reaction has not yet been completed. However, if obtained the new value might well be very different as it was for the $^{18}\text{C}(n,\gamma)^{19}\text{C}$ reaction. Hence, we have tested a large

range for this (α, n) reaction rate. Figure 11 shows the produced abundance sensitivity to the cross section ratio about the 2nd or 3rd peaks (left panel in Figure 11) and actinides (right panel in Figure 11). If the cross section increases by a factor of 100, the abundances of the 2nd and 3rd peaks are estimated to change by about 10%, while the actinides would change by about 30%.

In the range of $\lambda/\lambda_0 = 100$, the sensitivity of the (α, n) reaction is significant. On the other hand, in the range of $\lambda/\lambda_0 = [100 - 1000]$, the estimated abundance is almost constant (right side of Figure 11). In this region it has no sensitivity. This is because when the cross section for the (α, n) reaction becomes larger, it exceeds the rate for β -decay $\lambda_{18\text{C}(\alpha, n)^{21}\text{O}}/\lambda_\beta \geq 10$ throughout the nucleosynthesis process (see the lower panel of Figure 12). In this region, the (α, n) reaction plays a very important role because it determines whether the reaction flows through (α, n) or β -decay. However, in the range $\lambda/\lambda_0 = [100 - 1000]$, the order of the reaction flow speed between the (n, γ) , the (α, n) and the β -decay remains unchanged. The reaction flux stays at ^{18}C and only waits for the β -decay because the reaction flow of both (n, γ) and (α, n) reactions are much faster than β -decay. In essence, ^{18}C becomes a “semi-waiting point”. As a result, the reaction flow follows only one path that is $^{17}\text{C} \rightarrow ^{18}\text{C} \rightarrow ^{18}\text{N}$. Therefore the (α, n) rate does not affect the r-process. Hence, we find that the reaction $^{18}\text{C}(\alpha, n)^{21}\text{O}$ is most important for the r-process among all reactions on ^{18}C .

7. Summary and Conclusion

In this work, we have quantified the uncertainty of r-process nucleosynthesis to various light-element nuclear reactions. We checked the dependence of the sensitivities for several parameter sets in explosive environments (τ_{dyn} , s/k , Y_e and T_a). We found that knowing the dynamical timescale τ_{dyn} is most crucial for determining the reaction sensitivity for the light-element reactions studied here.

We identified the important reactions for the r-process by introducing the concept of sensitivity. The $\alpha(\alpha n, \gamma)^9\text{Be}$ reaction is the most important reaction regardless of the flow models, as has been noted previously. In the present work, however, we also identify other equally important reactions for synthesizing the r-process elements in SNe. They are primarily the $\alpha(t, \gamma)^7\text{Li}$ and $^7\text{Li}(n, \gamma)^8\text{Li}$ reactions, though other relatively important reactions were also found. We also carried out detailed analysis of the sensitivity for all other eighteen nuclear reactions by comparing the calculated results with the use of new experimental data and H.F. estimates. We have also analyzed the semi-waiting point at ^{18}C . An interesting feature of light-element waiting points is the importance of the competition between α -capture, neutron capture, and β -decay in the nuclear reaction flows for r-process nucle-

osynthesis. This applies generally to other light-mass nuclei such as ^8Li , ^{15}B , $^{16,18}\text{C}$, and ^{24}O , whose reaction Q-values or neutron capture rates are small. The only difference from the well studied waiting-point nuclei in heavier-mass regions (like ^{130}Cd and ^{132}Sn) is that α -capture is an additionally important flow which competes with neutron capture and β -decay in the light-mass region. This specific feature arises from the fact that the α -process, which proceeds prior to the neutron-capture flow on the intermediate-to-heavy mass nuclei, occurs at early times in the high temperature and high density of various expansion of the neutrino-driven wind.

We also studied extensively the dependence of the sensitivity on the expansion flow models. We adopted exponential flow models to simulate various expansion dynamics and calculated the sensitivity. The four important physical parameters which characterize the profile in the flow models are the dynamical timescale τ_{dyn} , the entropy per baryon s/k , the initial electron fraction Y_e , and the asymptotic temperature T_a . We found that the sensitivities depend most strongly on the dynamical timescale.

Nuclear reactions and SN dynamics are thus complementary facets to understanding r-process nucleosynthesis. Obviously, more accurate experimental data should help our comprehensive understanding of r-process nucleosynthesis and SN dynamics. We believe that the present work provides a useful tool to elucidate which reactions are most important and also the synergy between the SN dynamics and nuclear reactions in r-process nucleosynthesis.

This work has been supported in part by Grants-in-Aid for Scientific Research (13640313) and for Specially Promoted Research (13002001) of the Ministry of Education, Science, Sports and Culture of Japan, and The Mitsubishi Foundation. Work at The University of Notre Dame has been supported under DoE nuclear theory grant DE-FG02-95-ER 40934.

8. Appendix A

8.1. Justification of the Incoherent Approximation for α_i

We have discussed the reaction sensitivity by making the incoherent approximation, Eq. (7), assuming that α_i is most sensitive to the change of the corresponding i -th nuclear reaction rate λ_i and that its dependence on different λ_j 's ($j \neq i$) is weak. In order to justify this approximation quantitatively, we carried out several calculations of α_i by changing two or three reaction rates $\{\lambda_j\}$ simultaneously. For this purpose we chose the three most important nuclear reactions from Tables 7 and 8, i.e. (1) $\alpha(\alpha n, \gamma)^9\text{Be}$, (2) $\alpha(t, \gamma)^7\text{Li}$, and (3) $^7\text{Li}(n, \gamma)^8\text{Li}$. These reactions show fairly large absolute values of the sensitivity parameter

α_i .

Figure 13 displays the calculated r-process yields, in which we have changed the three reaction rates as indicated. Solid curves show the results of the exact calculation and the dotted curves show the results of making the incoherent approximation

$$\frac{Y_r}{Y_r(0)} \simeq \left(\frac{\lambda_1}{\lambda_1(0)} \right)^{\alpha_1} \left(\frac{\lambda_2}{\lambda_2(0)} \right)^{\alpha_2} \left(\frac{\lambda_3}{\lambda_3(0)} \right)^{\alpha_3}, \quad (23)$$

where the α_i 's are taken from Table 7 for the fast wind model. The exact (solid) and approximate (dotted) calculations are in reasonable agreement with each other for the r-process abundances in the 2nd and 3rd peaks. A large deviation, however, emerges in actinide elements when the three reaction rates are set to near the lower limits of the estimated uncertainties of the cross sections.

These results indicate that the incoherent approximation is a fairly good approximation, except for the actinide elements. We attribute this deviation for actinide nuclei to the fact that the three most important reactions change the neutron-to-seed ratio in slightly different manners. This enhances the sensitivity in the actinide production near the end of the neutron-capture flow along the r-process path. (See Table 7 and Otsuki et al. 2003.)

REFERENCES

- Adelberger, E.G., et al. 1998, Rev. Mod. Phys. 70, 1265.
- Angulo, C. et al. 1999, Nucl. Phys. A656, 3 (NACRE)
- Arlandini, C., Kaeppler, F., Wisshak, K., Gallino, R., Lugaro, M., & Straniero, O. 1999, ApJ, 525, 886.
- Bahcall, J. N., Huebner, W. F., Lubow, S. H., Parker, P. D., & Ulrich, R. K. 1982, Rev. Mod. Phys., 54, 767 767
- Beer, H., Wiescher, M., Kaeppler, F., Goerres, J., & Koehler, P. E. 1992, ApJ, 387, 258
- Boyd, R.N. & Kajino, T. 1989, ApJ 336, L55.
- Boyd, R.N. et al. 1992, Phys. Rev. Lett. 68, 1283.
- Brune, C. R., Kavanagh, R. W., & Rolfs, C. 1994, Phys. Rev. C, 50, 2205.
- Buchmann, L., Gete, E., Chow, J. C., King, J. D., & Measday, D. F. 2001, Phys. Rev. C63, 034303

- Cameron, A. G. W. 2001, *ApJ*, 562, 456
- Cameron, A. G. W. 2003, *ApJ*, 587, 327
- Cardall, C. Y. & Fuller, G. M. 1997, *ApJ*, 486, L111
- Caughlan, G. R., & Fowler, W. A. 1988, *Atomic Data and Nuclear Data Tables*, 40, 283 (CF88)
- Cowan, J. J., McWilliam, A., Sneden, C., & Burris, D. L. 1997, *ApJ*, 480, 246
- Delano, M. D., & Cameron, A. G. W. 1971, *Ap&SS*, 10, 203
- Descouvemont, P. 2002, *Nuclear Physics A*, 699, 463
- Descouvemont, P. et al. 2004, *Atomic Data and Nuclear Data Tables*, 88, 203. (ADNDT04)
- Freiburghaus, C., Rosswog, S., & Thielemann, F.-K. 1999, *ApJ*, 525, L121
- Fujimoto, S., Hashimoto, M., Arai, K., & Matsuba, R. 2004, *ApJ*, 614, 847
- Fukuda, N. et al. 2004, *Phys. Rev. C* 70, 054606.
- Gibbons, J.H., et al. 1961, *Phys. Rev.* 122,182.
- Gu, X. et al. 1995, *Phys. Rev. Lett.* B343, 31.
- Hillebrandt, W., Wolff, R. G., & Nomoto, K. 1984, *A&A*, 133, 175
- Ishiyama, T., et al., 2004, *IAP Conf. Proc.* 704, 453.
- Hoffman, R. D., Woosley, S. E., & Qian, Y.-Z. 1997, *ApJ*, 482, 951
- Honda, S., Aoki, W., Kajino, T., Ando, H., Beers, T. C., Izumiura, H., Sadakane, K., & Takada-Hidai, M. 2004, *ApJ*, 607, 474
- Horváth, Á., et al. 2002, *ApJ*, 570, 926
- Inoue, S., Iwamoto, N., Orito, M., & Terasawa, M. 2003, *ApJ*, 595, 294
- Kajino, T. 1986, *Nucl. Phys.* A460, 559.
- Kajino, T. & Boyd, R.N. 1990, *ApJ* 359, 267.
- Kajino, T., Mathews, G. J., & Fuller, G. M. 1990, *ApJ*, 364, 7
- Kajino, T., Toki, H., & Austin, S. M. 1987, *ApJ* 319, 531.

- Kajino, T., Wanajo, S., & Mathews, G. J. 2002, Nuclear Physics A, 704, 165
- Kikuchi, T., Nagai, Y., Suzuki, T. S., Shima, T., Kii, T., Igashira, M., Mengoni, A., & Otsuka, T. 1998, Phys. Rev. C, 57, 2724
- Macklin, R. L. 1990, ApJ, 357, 649
- Malaney, R.A. & Fowler, W.A. 1988, ApJ 333, 14.
- Mathews, G. J. & Cowan, J. J. 1990, Nature, 345, 491
- Mathews, G. J., Mengoni, A., Thielemann, F.-K. & Fowler, W. A. 1983, ApJ, 270, 740
- Meyer, B. S. 1995, ApJ, 449, L55
- Meyer, B. S. & Brown, J. S. 1997, ApJS, 112, 199
- Meyer, B. S., Mathews, G. J., Howard, W. M., Woosley, S. E., & Hoffman, R. D. 1992, ApJ, 399, 656
- Mughabghab, S.F., Divadeenam, M., & Holden, N.E. 1981, Neutron Cross Section, vol.1 (New York : Academic).
- Mizoi, et al. 2000, Phys. Rev. C62, 065801.
- Mukha et al. 2005, Nucl. Phys. A, in press.
- Nagai, Y. et al. 1991a, ApJ 372, 683
- Nagai, Y. et al. 1991b, ApJ 381, 444
- Nakamura, T. et al. 1999, Phys. Rev. Lett. 83, 1112
- Nakamura, T., et al. 1994, Physics Letters B, 331, 296
- Nakamura, T., et al. 2003, Nuclear Physics A, 722, 301C
- Nollett, K. M., & Burles, S. 2000, Phys. Rev. D, 61, 123505
- Ohsaki, T., Nagai, Y., Igashira, M., Shima, T., Takeda, K., Seino, S., & Irie, T. 1994, ApJ, 422, 912
- Orito, M., Kajino, T., Boyd, R. N., & Mathews, G. J. 1997, ApJ, 488, 515
- Otsuki, K., Tagoshi, H., Kajino, T., & Wanajo, S. 2000, ApJ, 533, 424

- Otsuki, K., Mathews, G. J., & Kajino, T. 2003, *New Astronomy*, 8, 767
- Paradellis, T. et al. 1990, *Z. Phys.* A337, 211.
- Pramanik, U.D. et al. 2003, *Phys. Lett.* B551, 63.
- Pruet, J., Woosley, S. E., & Hoffman, R. D. 2003, *ApJ*, 586, 1254
- Qian, Y.-Z. & Wasserburg, G.J. 2000, *Phys. Rep.* 333,77
- Qian, Y.-Z. & Woosley, S. E. 1996, *ApJ*, 471, 331
- Raman, S., Igashira, M., Dozono, Y., Kitazawa, H., Mizumoto, M., & Lynn, J. E. 1990, *Phys. Rev. C*, 41, 458
- Rauscher, T., Applegate, J. H., Cowan, J. J., Thielemann, F., & Wiescher, M. 1994, *ApJ*, 429, 499
- Sasaqui, T., Kajino, T. & Balantekin, A.B. 2005, *ApJ*, to be submitted.
- Schatz, H., Toenjes, R., Pfeiffer, B., Beers, T. C., Cowan, J. J., Hill, V., & Kratz, K. 2002, *ApJ*, 579, 626
- Smith, M.S., Kawano, L.H., & Malaney, R.A. 1993, *ApJS*, 85, 219
- Snedden, C., McWilliam, A., Preston, G. W., Cowan, J. J., Burr's, D. L., & Armosky, B. J. 1996, *ApJ*, 467, 819
- Sumiyoshi, K., Suzuki, H., Otsuki, K., Terasawa, M., & Yamada, S. 2000, *PASJ*, 52, 601
- Sumiyoshi, K., Terasawa, M., Mathews, G. J., Kajino, T., Yamada, S., & Suzuki, H. 2001, *ApJ*, 562, 880
- Sumiyoshi, K., Utsunomiya, H., Goko, S., & Kajino, T. 2002, *NP A719*, 467-486
- Takahashi, K. & Janka, H.-T. 1997, Origin of matter and evolution of galaxies in the universe '96. Proceedings of an international conference held in Atami, Japan, 18-20 January 1996, (Singapore: World Scientific, 1997), edited by T. Kajino, Y. Yoshii, and S. Kubono, p. 213.
- Terasawa, M., Sumiyoshi, K., Kajino, T., Mathews, G. J., & Tanihata, I. 2001, *ApJ*, 562, 470
- Terasawa, M., Sumiyoshi, K., Yamada, S., Suzuki, H., & Kajino, T. 2002, *ApJ*, 578, L137

- Thompson, T., Burrows, A. & Meyer, B. S. 2001, *ApJ*, 562, 887
- Utsunomiya, H., et al. 2001, *Phys. Rev. C*63, 018801
- Wanajo, S., Kajino, T., Mathews, G. J., & Otsuki, K. 2001, *ApJ*, 554, 578
- Wanajo, S., Itoh, N., Ishimaru, Y., Nozawa, S., & Beers, T. C. 2002, *ApJ*, 577, 853
- Wanajo, S., Tamamura, M., Itoh, N., Nomoto, K., Ishimaru, Y., Beers, T. C., & Nozawa, S. 2003, *ApJ*, 593, 968
- Wiescher, M., Steininger, R., & Kaeppler, F. 1989, *ApJ*, 344, 464
- Wiescher, M., Gorres, J., & Thielemann, F. 1990, *ApJ*, 363, 340
- Wilson, J. R., Mayle, R. W., 1993, *Phys. Rep.*, 227, 97
- Witti, J., Janka, H.-T., & Takahashi, K. 1994, *A&A*, 286, 841
- Woosley, S. E., & Hoffman, R. D. 1992, *ApJ*, 395, 202
- Woosley, S. E., Wilson, J. R., Mathews, G. J., Hoffman, R. D., & Meyer, B. S. 1994, *ApJ*, 433, 229

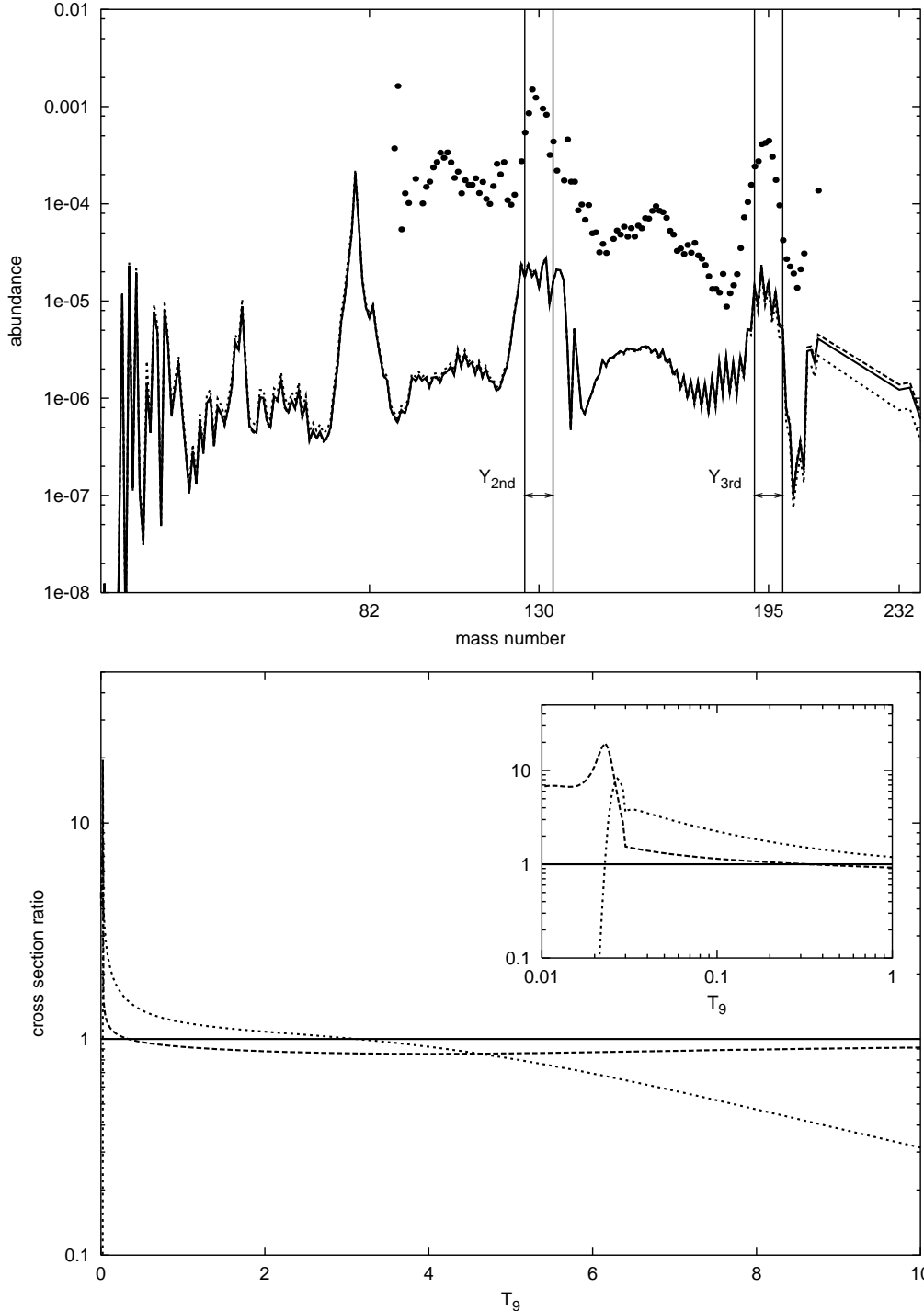


Fig. 1.— The upper panel shows a comparison of the final r-process abundances obtained with different $\alpha(\alpha n, \gamma)^9\text{Be}$ reaction rates. Dotted line is for the rate of Woosley and Hoffman 1992 (which agrees with that of Caughlan and Fowler (1988) within 30 %), the dashed line is for the rate of the NACRE compilation (Angulo et al. 1999), and the solid line is for the rate of Utsumomiya et al. (2001) and Sumiyoshi et al. (2002). Y_{2nd} and Y_{3rd} indicate the typical r-process abundances of the 2nd peak and 3rd peak elements, respectively. The solar system r-process abundances from Arlandini et al. (1999) are shown by filled circles. The lower panel shows the reaction rates as a function of temperature, T_9 , as explained above. Inset

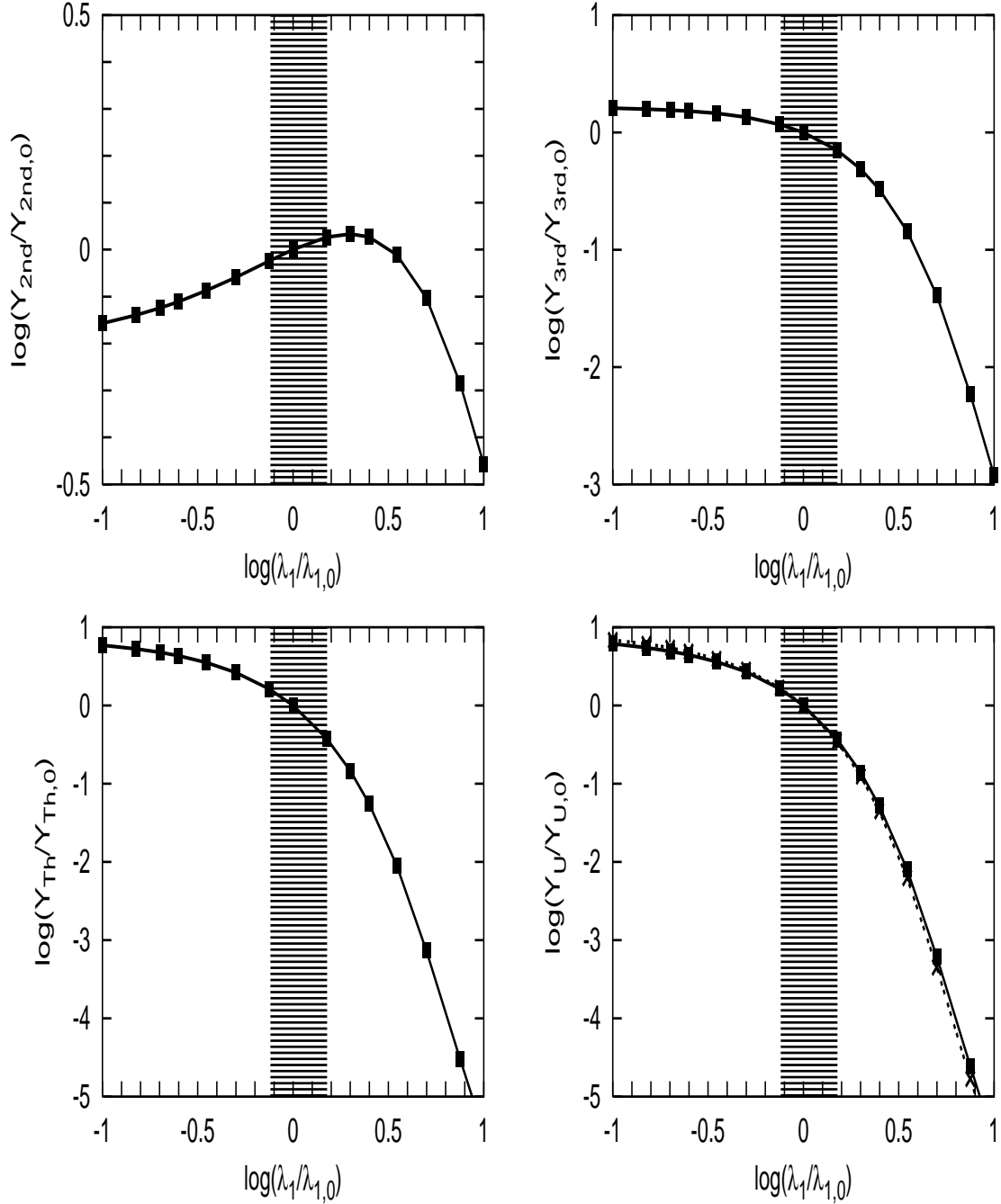


Fig. 2.— Abundance ratios of the 2nd-peak (upper left), 3rd-peak (upper right), Th (lower left), and U (lower right) elements relative to the original abundances as a function of $\lambda_1/\lambda_{1,0}$ for the $\alpha(\alpha n, \gamma)^9\text{Be}$ reaction (1) in Table 1. Solid lines show the best fit to these data based on Eq.(7). Note that the solid and dotted lines for U (lower right) are for ^{235}U and ^{238}U , respectively. The shaded areas indicate the adopted uncertainties in the nuclear reaction rate tabulated in Table 1.

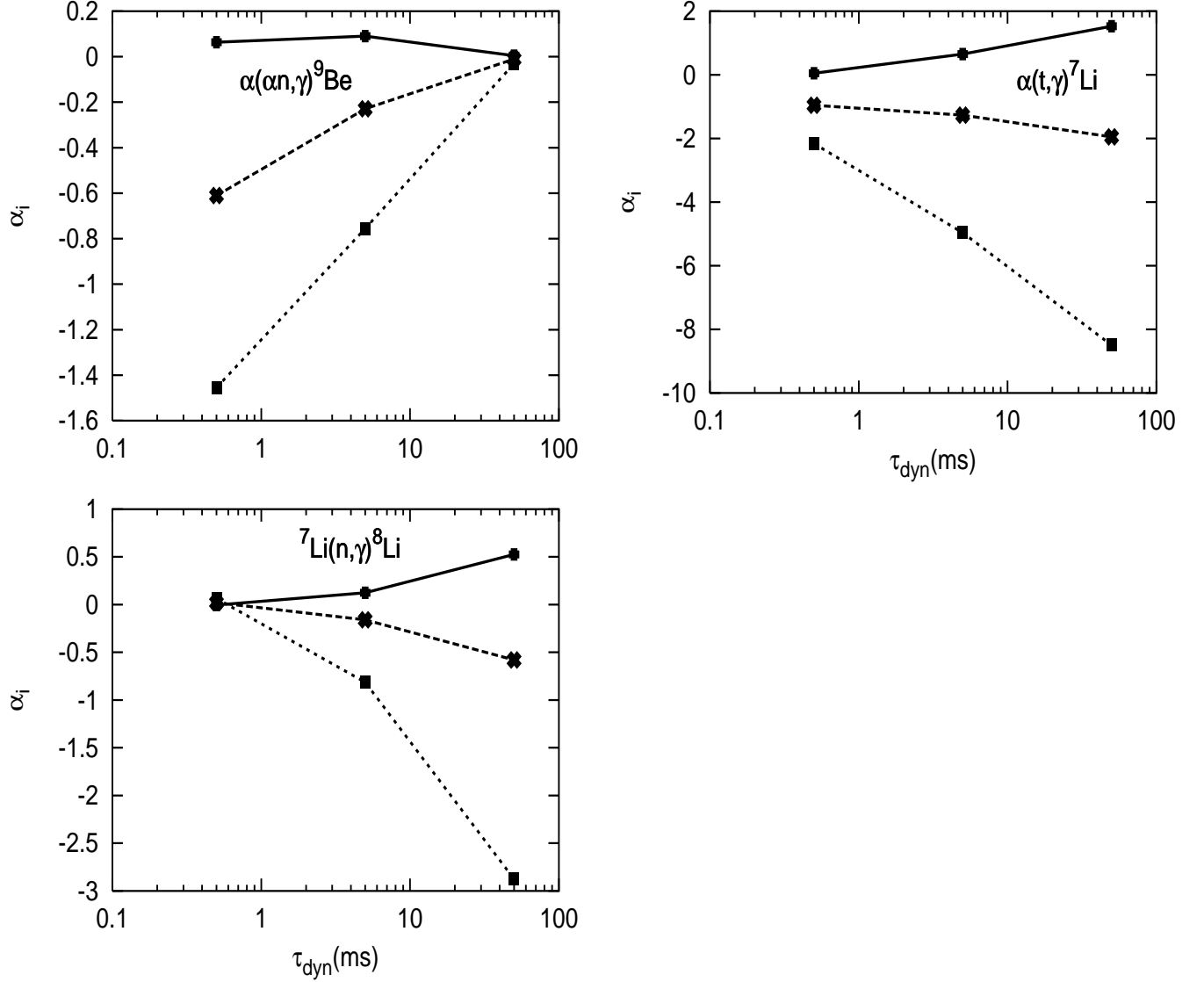


Fig. 3.— Dependence of the sensitivity parameter, α_i , on the dynamical timescale, τ_{dyn} , for the 2nd-peak (solid line and thick-plus points), 3rd-peak (dashed line and thick-cross points), and actinide (dotted line and square points) elements, corresponding to the parameter sets given in Table 3. α_i for actinide elements is the simple average of those for ${}^{232}\text{Th}$, ${}^{235}\text{U}$, and ${}^{238}\text{U}$. The top left is for $\alpha(\alpha n, \gamma){}^9\text{Be}$, the top right is for $\alpha(t, \gamma){}^7\text{Li}$, and the lower is for ${}^7\text{Li}(n, \gamma){}^8\text{Li}$.

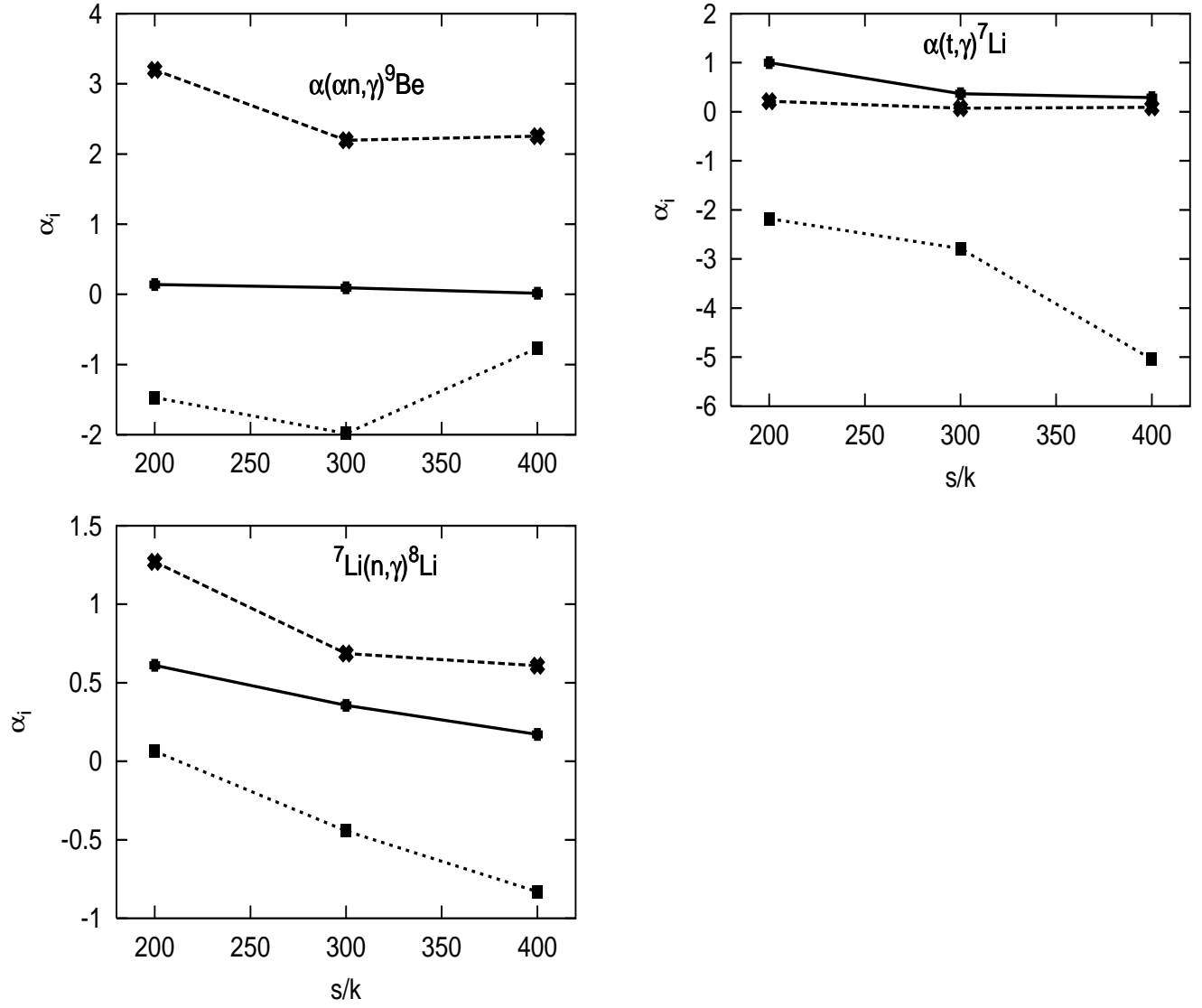


Fig. 4.— Dependence of the sensitivity parameter, α_i , on the entropy per baryon, s/k , corresponding to the parameter sets in Table 4. Three symbols are the same as those in Fig. 3. The dependence on s/k is very small, except for actinide elements (squares).

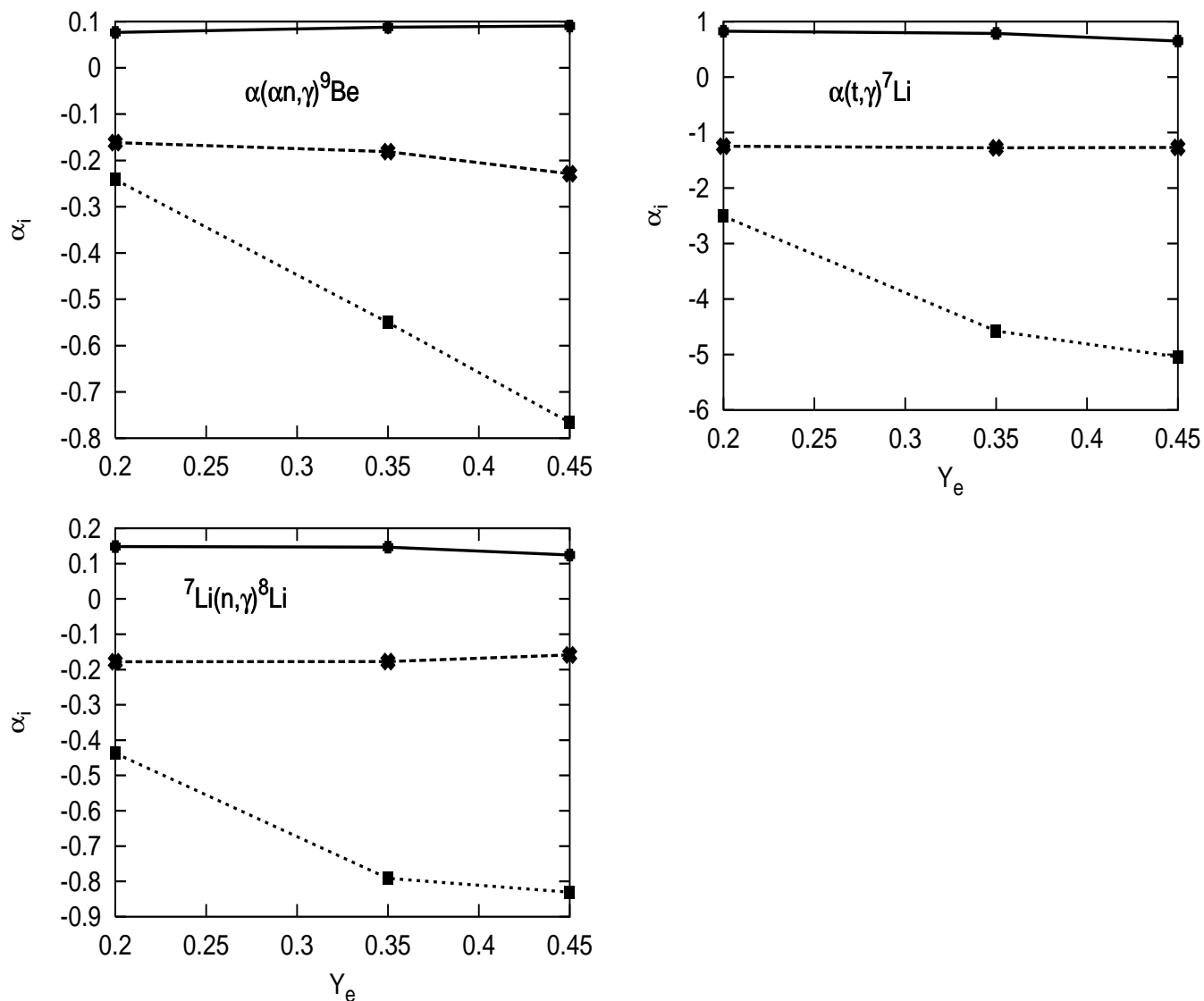


Fig. 5.— Dependence of the sensitivity parameter, α_i , on the initial electron fraction, Y_e , corresponding to the parameter sets given in Table 5. Three symbols are the same as those in Fig.3. The dependence on Y_e is very small, except for actinide elements (squares).

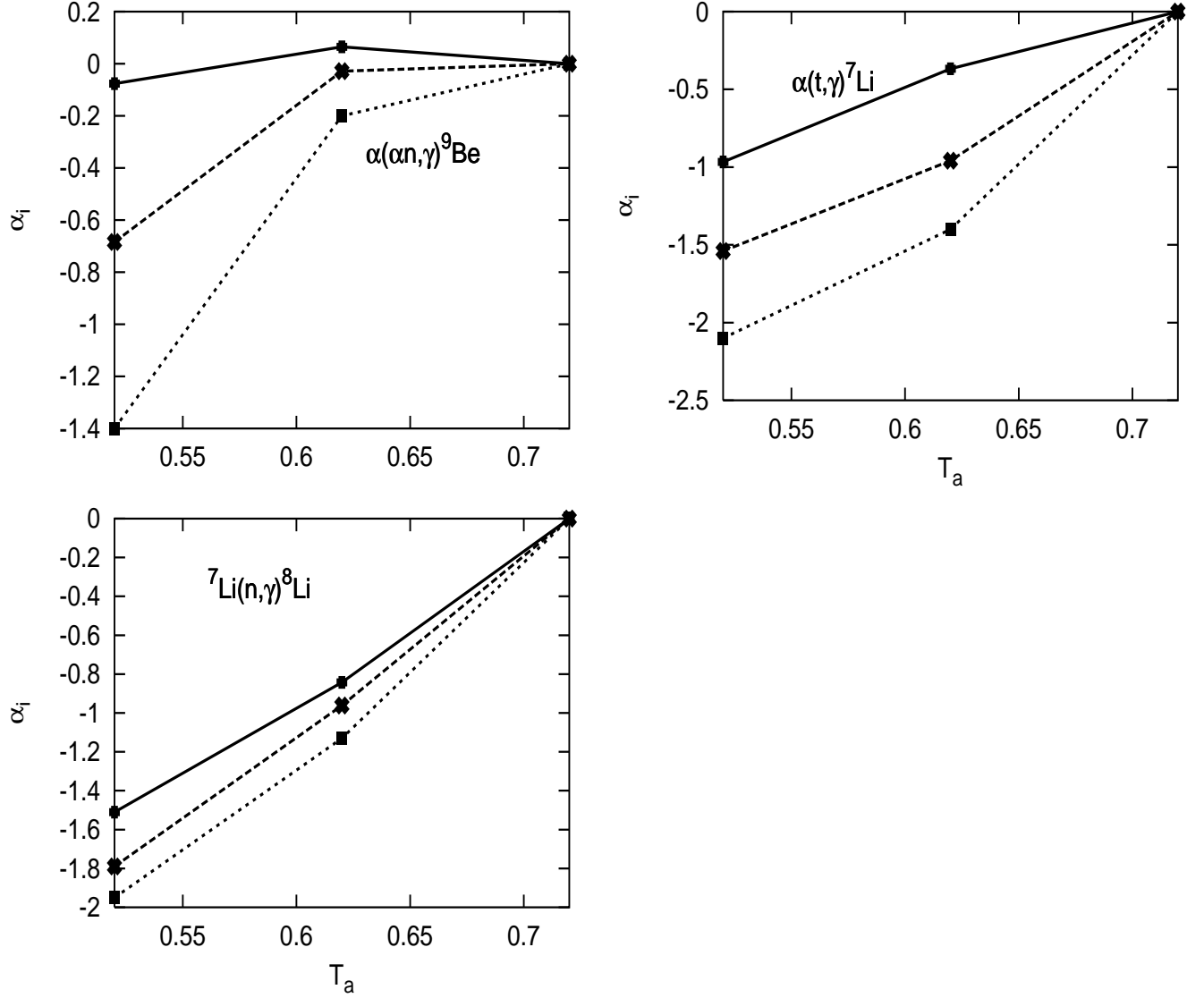


Fig. 6.— Dependence of the sensitivity parameter, α_i , on the asymptotic temperature, T_a , corresponding to the parameter sets given in Table 6. Three symbols are the same as those in Fig.3. The dependence on T_a is strong, but weaker than the dependence on τ_{dyn} (see Fig. 3).

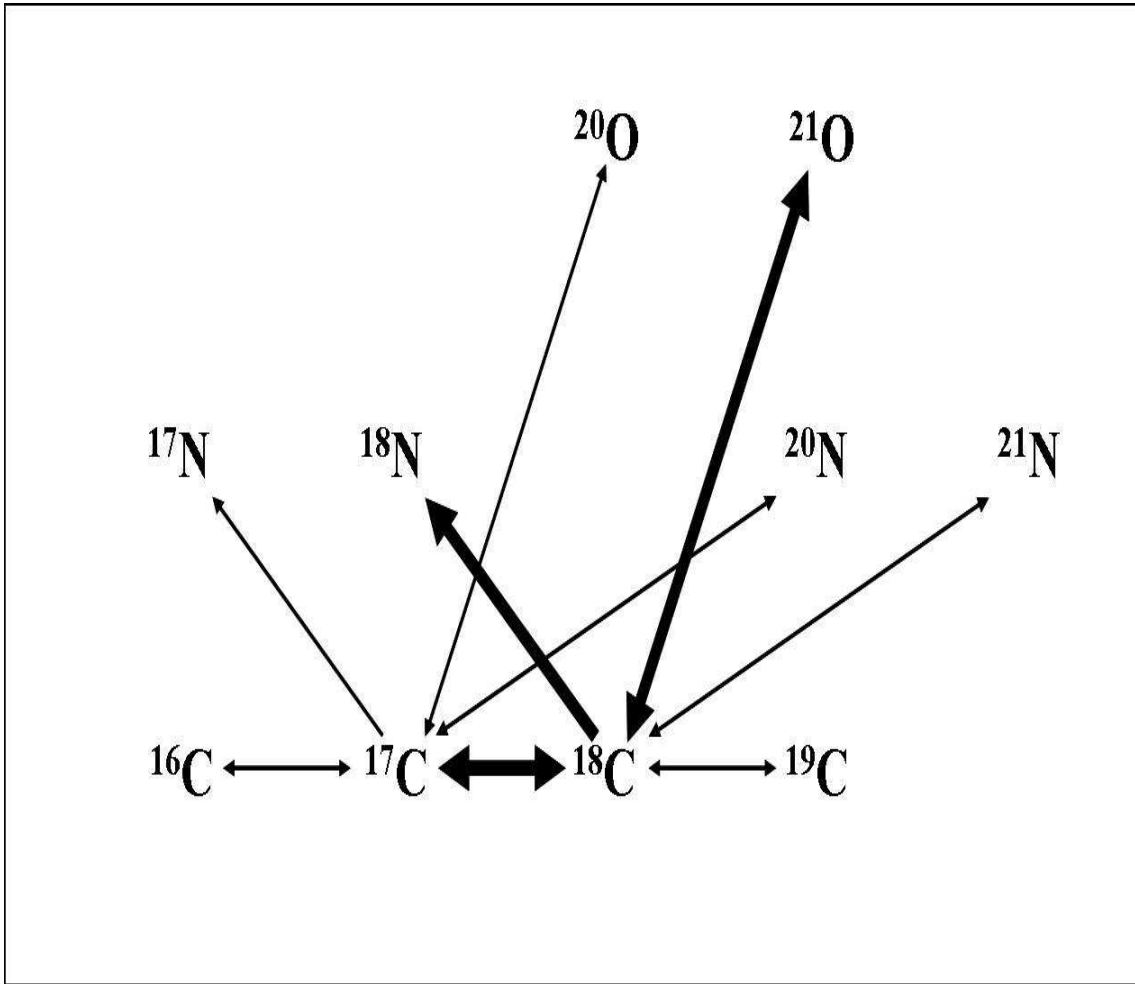


Fig. 7.— The reaction flows near ^{18}C . The thick arrows indicate the most important reactions, which lead to finite sensitivities in the r-process nucleosynthesis shown in Tables 7 - 13.

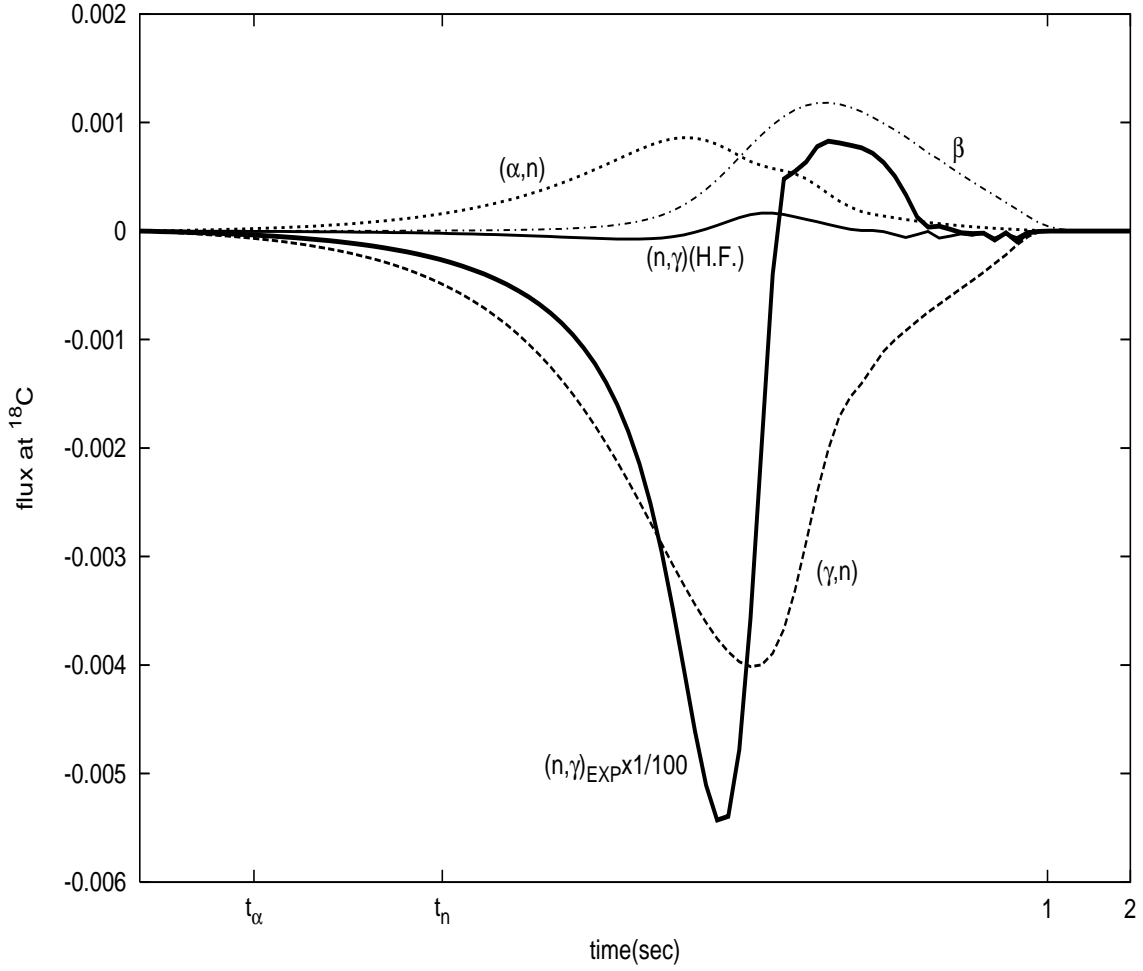


Fig. 8.— Net nuclear flux through ^{18}C as a function of time, Eq.(16). Positive values denote flux out of ^{18}C , while negative values denote flux flowing into ^{18}C . t_α indicates the time at which NSE breaks down and the α -process effectively begins. t_n is the time at which the α -process freezes out and n-captures begin. The solid lines show the $^{18}\text{C}(n, \gamma)^{19}\text{C}$ flow when the HF estimate (thin solid line) or the experimental data (thick solid line) were used as labeled. The dotted line, the dot-dash line, and the dash line express the $^{18}\text{C}(\alpha, n)$, β -decay, and $^{18}\text{C}(\gamma, n)$ flows, respectively. Note that the (n, γ) and (γ, n) rates always dominate over the (α, n) and β -decay rates. With the HF estimates, however, the n-capture reactions are ineffective, so that α -capture and β -decay processes balance the photo-disintegration. With the experimental rate, n-capture dominates the other three reactions. Even so, most of the flux flows to ^{18}C so that it becomes a new “semi-waiting” point (see text in Sect. 6.2 in detail).

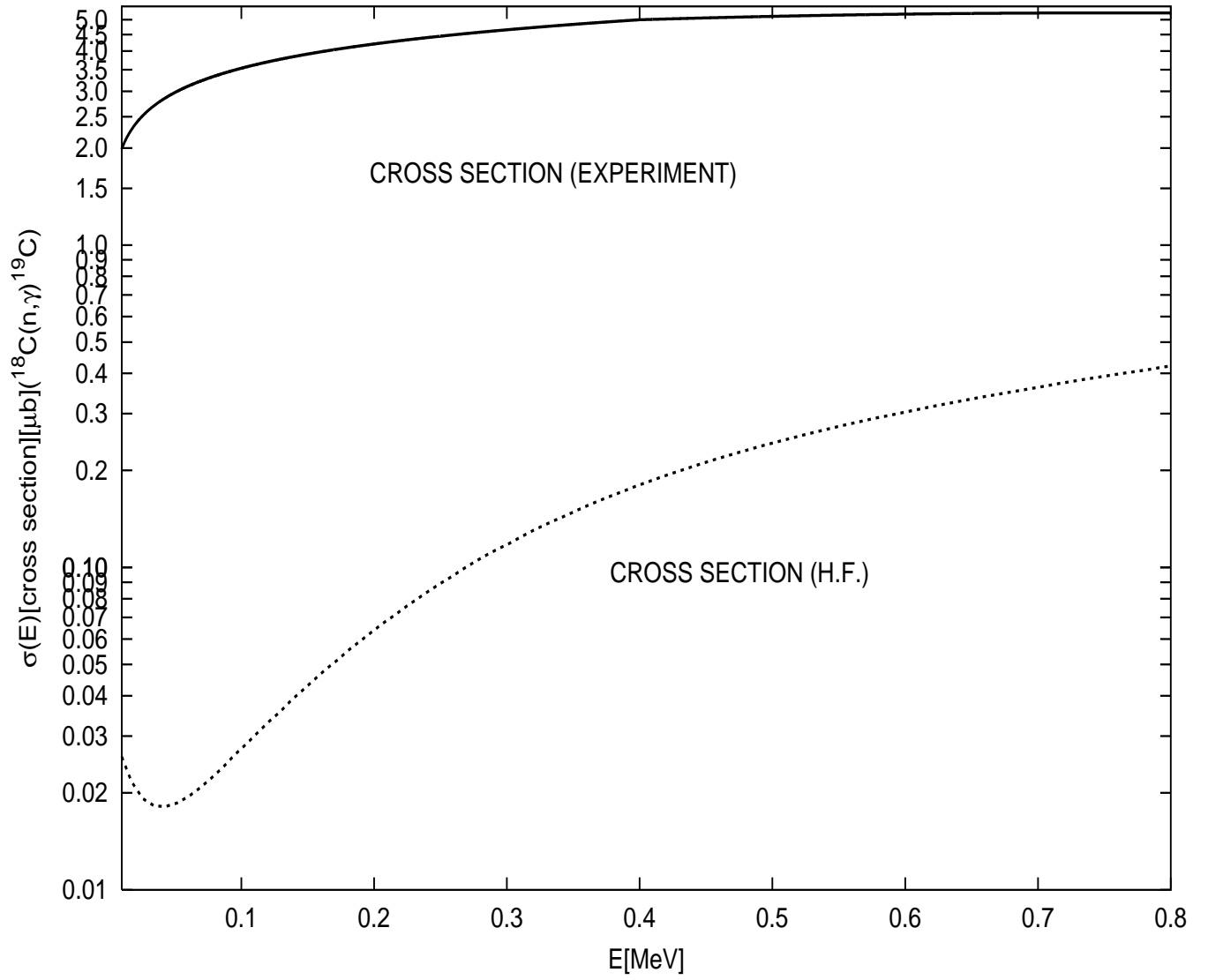


Fig. 9.— Comparison of the experimentally determined $^{18}\text{C}(n,\gamma)^{19}\text{C}$ cross section (solid line) of Nakamura et al. (1999) with Hanser-Feshbach estimates (dotted line).

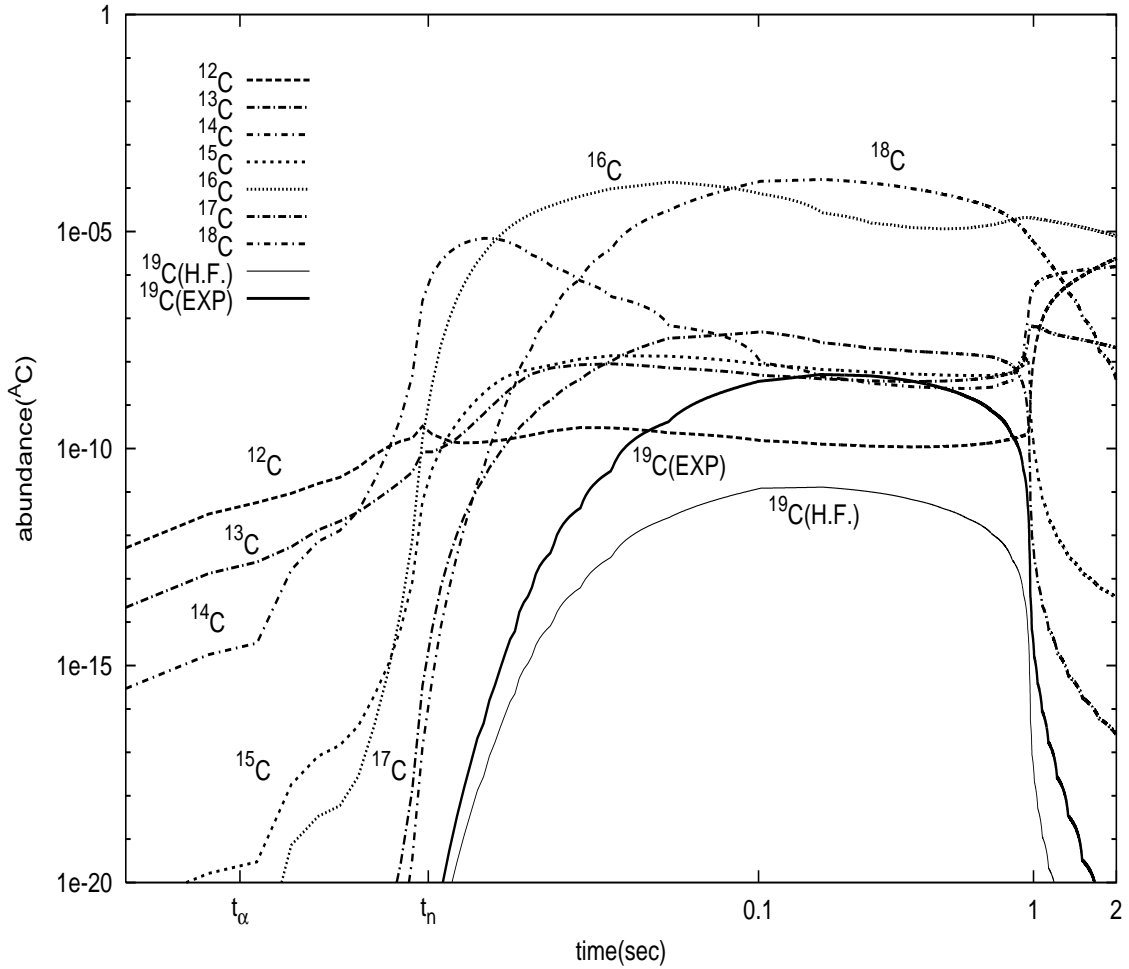


Fig. 10.— Time evolution of carbon isotope abundances. Because of the large measured reaction cross section for $^{18}\text{C}(n,\gamma)^{19}\text{C}$, the abundance of ^{19}C is increased compared with the abundance based upon the HF estimate (see Figure 9). However, the sensitivity of this reaction to the r-process is small (see Table 7). The accumulated abundance of ^{19}C rapidly photodisintegrates to ^{18}C due to the small neutron-separation energy (see Table 3 and text).

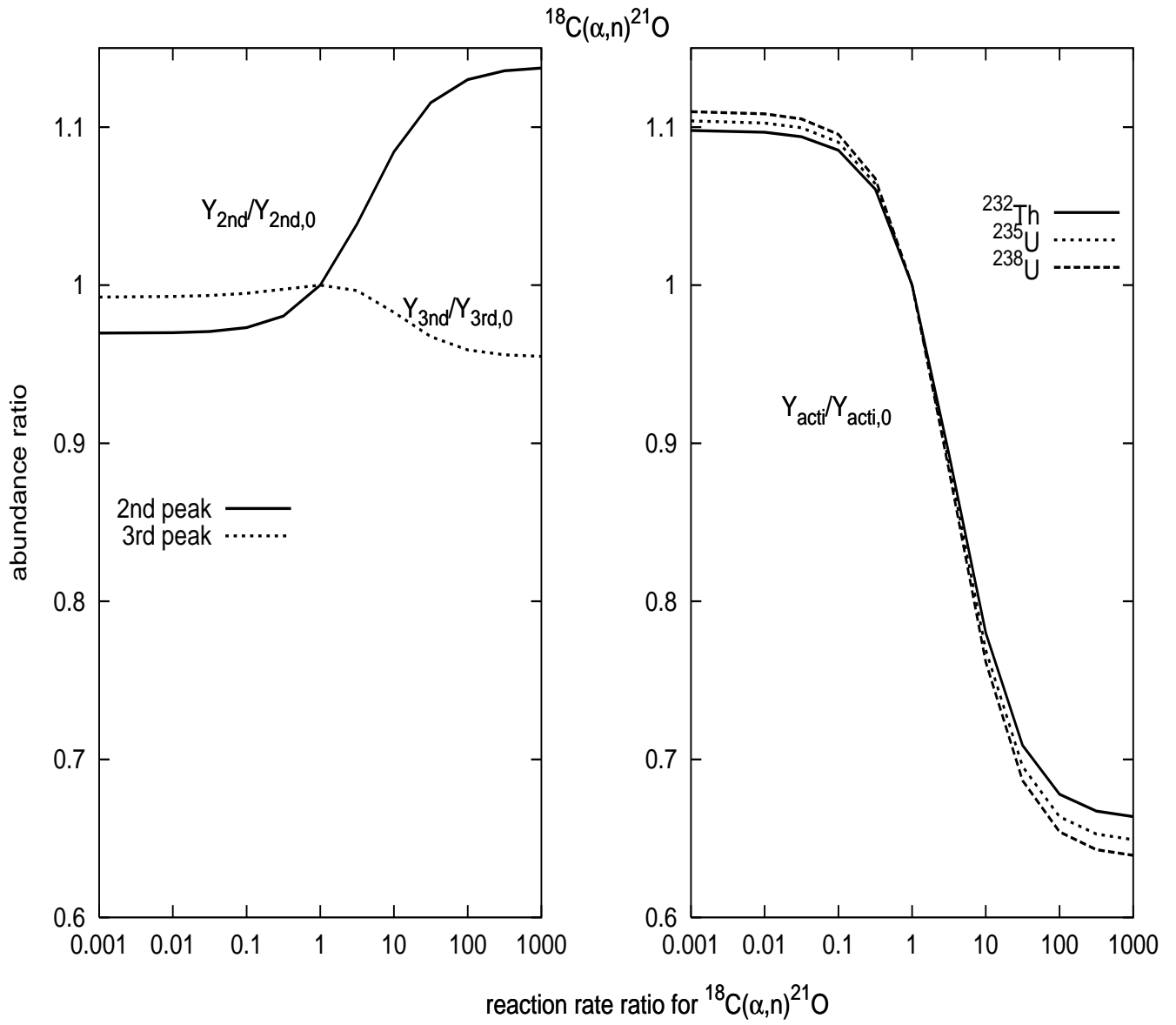


Fig. 11.— Calculated abundance ratios for the 2nd or 3rd peak (left) and actinide (right) elements as a function of the reaction rate $\lambda_i/\lambda_i(0)$ for $^{18}\text{C}(\alpha,n)^{21}\text{O}$.

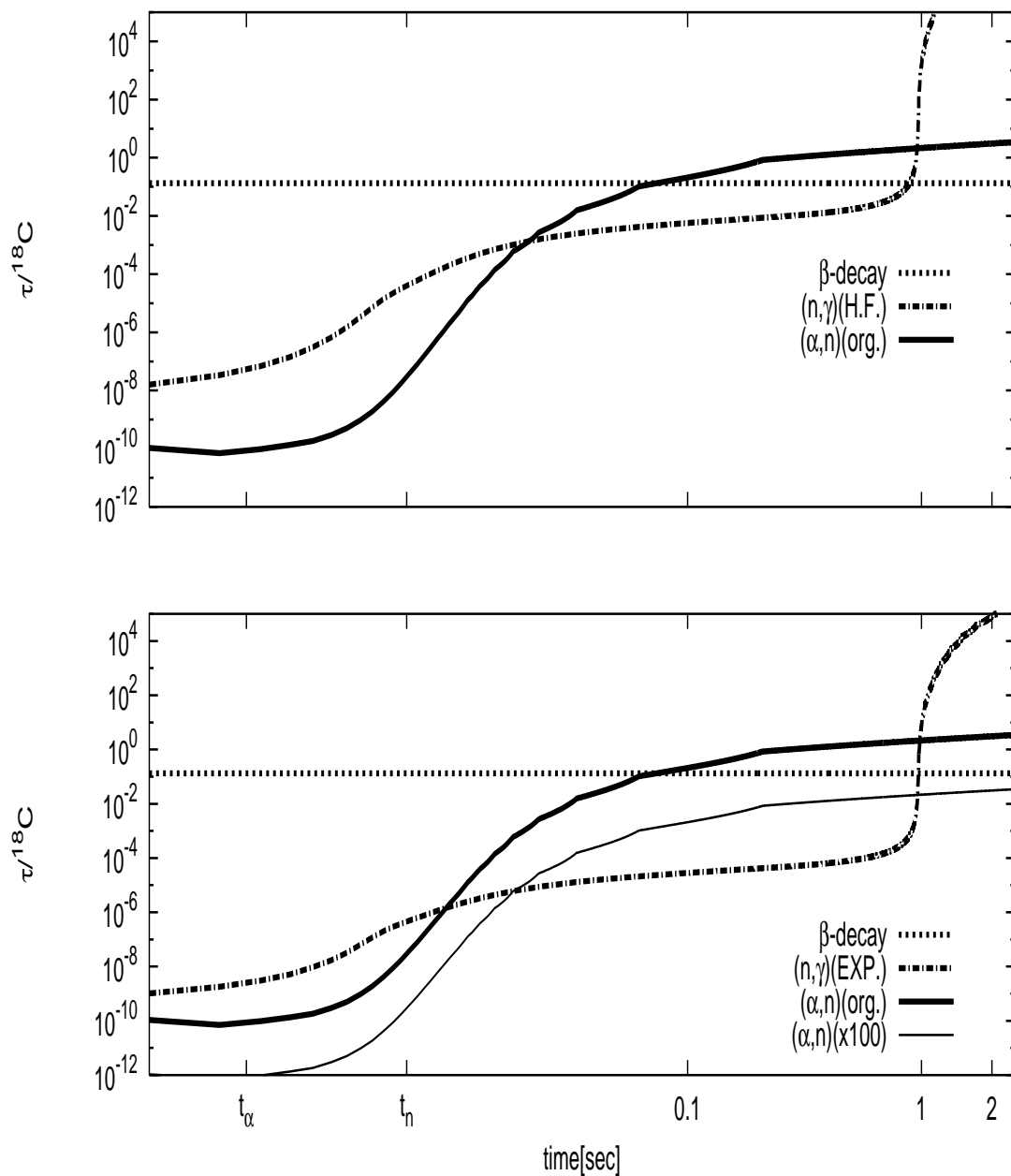


Fig. 12.— Reaction time scales per ^{18}C for (n,γ) , (α,n) and β -decay. The top panel shows the result based upon HF estimates for the (n,γ) reaction rate. The lower panel shows the result of using the experimental (n,γ) rate. For illustration, the lower panel also shows the result of changing the (α,n) cross section by a factor of 100. Increasing the (α,n) cross section leads to a change of the order of the reaction flow speed through (α,n) . t_α and t_n are the same as those in Figure 8.

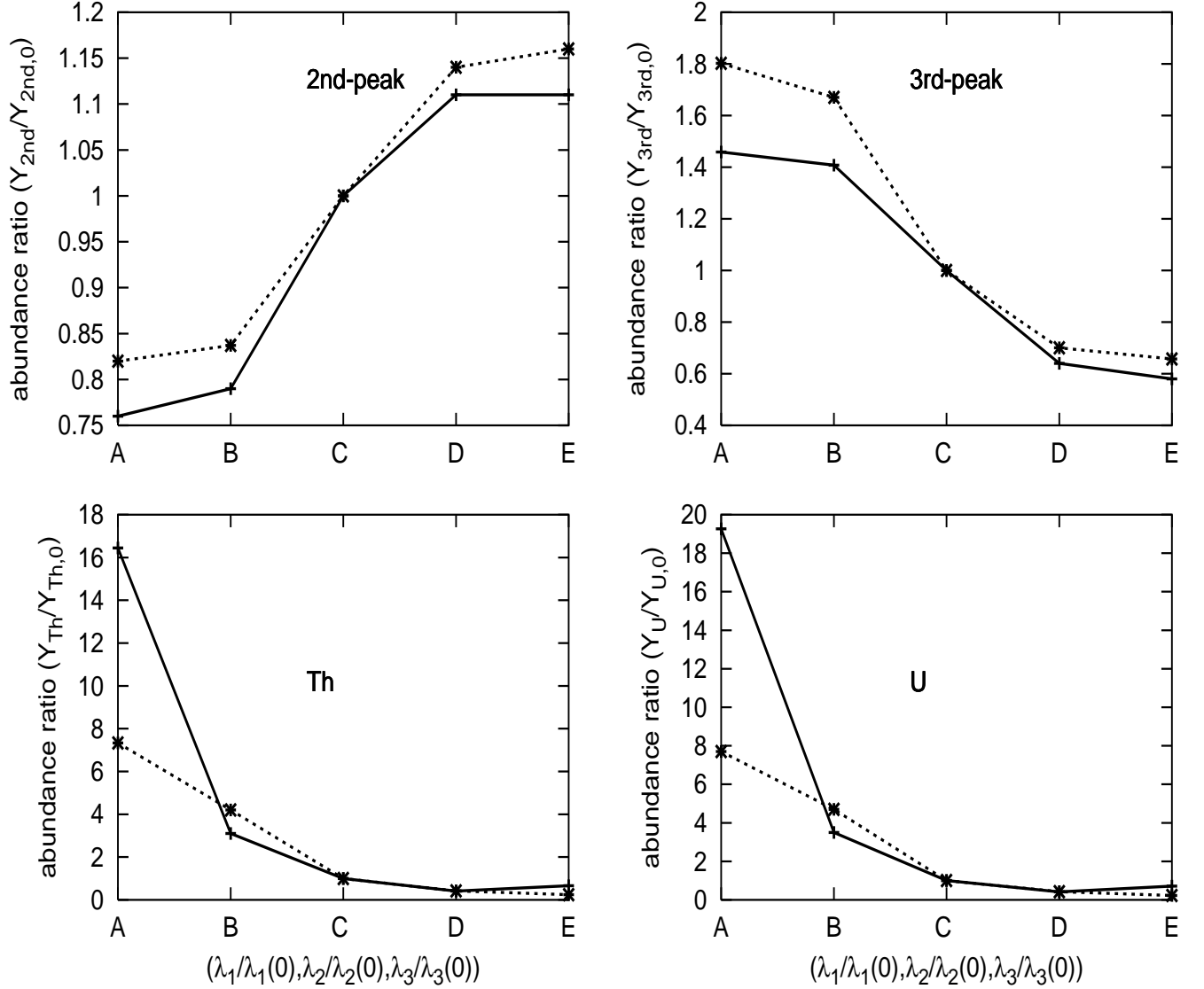


Fig. 13.— Calculated r-process yields for the triple variation of reaction rates. Solid curves show the exact calculation, while the dotted curves are based upon the incoherent approximation, Eq.(7). The points 'A', 'B', 'C', 'D', and 'E' corresponds to $(\lambda_1/\lambda_1(0), \lambda_2/\lambda_2(0), \lambda_3/\lambda_3(0)) = (0.65, 0.70, 0.65), (0.65, 0.70, 1.0), (1.0, 1.0, 1.0), (1.35, 1.30, 1.0),$ and $(1.35, 1.30, 1.35)$, respectively.

Table 1: The most important 18 light-mass nuclear reactions, adopted 'standard' thermonuclear reaction rates, $\lambda_i(0)$, and uncertainties.

reactions	$N_A \langle \sigma v \rangle$	$1\sigma^b$	refs. ^c
(1) $\alpha(\alpha n, \gamma)^9\text{Be}$	$N_A^2 \langle \alpha \alpha n \rangle = 2.43 \times 10^9 T_9^{-2/3} \exp\{-13.490 T_9^{-1/3} - (T_9/0.15)^2\} \times (1 + 74.5 T_9) + 6.09 \times 10^5 T_9^{-3/2} \exp(-1.054/T_9) \times [1 - 58.80 T_9 - 1.794 \times 10^4 T_9^2 + 2.969 \times 10^6 T_9^3 - 1.535 \times 10^8 T_9^4 + 2.610 \times 10^9 T_9^5]$	$\pm 35\%$	Sumiyoshi et al. 2002
(2) ^a $\alpha(t, \gamma)^7\text{Li}$	$3.032 \times 10^5 T_9^{-2/3} \exp(-8.09/T_9^{1/3}) [1.0 + 0.0516 T_9^{1/3} + 0.0229 T_9^{2/3} + 8.28 \times 10^{-3} T_9 - 3.28 \times 10^{-04} T_9^{4/3} - 3.01 \times 10^{-04} T_9^{5/3}] + 5.109 \times 10^5 T_{9*}^{5/6} T_9^{-3/2} \exp(-8.068/T_{9*}^{1/3})$	$\pm 30\%$	Kajino et al. 1987
(3) $^7\text{Li}(n, \gamma)^8\text{Li}$	$4.90 \times 10^3 + 9.96 \times 10^3 T_9^{-3/2} \exp(-2.62/T_9)$	$\pm 35\%$	Nagai et al. 1991b
(4) $^8\text{Li}(\alpha, n)^{11}\text{B}$	$4.929 \times 10^6 T_9^{-3/2} \exp(-4.410/T_9) + 5.657 \times 10^8 T_9^{-3/2} \exp(-6.846/T_9) + 4.817 \times 10^9 T_9^{-3/2} \exp(-11.836/T_9) + 1.0 \times 10^{12} (10.03 T_9^{-1} + 4.814 T_9^{-2/3}) \exp(-19.45/T_9^{1/3})$	$\times 2$	X.Gu et al. 1995
(5) $^9\text{Be}(n, \gamma)^{10}\text{Be}$	$1.01 \times 10^3 + 1.01 \times 10^4 T_9^{-3/2} \exp(-6.487/T_9) + 5.41 \times 10^4 T_9^{-3/2} \exp(-8.471/T_9)$	$\times 2$	Rauscher et al. 1994
(6) $^{11}\text{B}(n, \gamma)^{12}\text{B}$	$7.38 \times 10^2 + 3.86 \times 10^3 T_9^{-3/2} \exp(-0.244/T_9) + 3.34 \times 10^4 T_9^{-3/2} \exp(-4.99/T_9)$	$\times 2$	Rauscher et al. 1994
(7) $^{12}\text{B}(n, \gamma)^{13}\text{B}$	$1.7 \times 10^3 + 9.548 \times 10^3 T_9^{-3/2} \exp(-1.625/T_9) + 1.562 \times 10^3 T_9^{-3/2} \exp(-2.666/T_9) + 1.163 \times 10^4 T_9^{-3/2} \exp(-5.919/T_9)$	$\times 2$	Rauscher et al. 1994
(8) $^{13}\text{B}(n, \gamma)^{14}\text{B}$	$1.02 \times 10^1 + 4.950 \times 10^1 T_9 + 4.940 \times 10^4 T_9^{-3/2} \exp(-4.76/T_9)$	$\times 2$	Rauscher et al. 1994
(9) $^{14}\text{B}(n, \gamma)^{15}\text{B}$	$1.906 \times 10^3 + 1.142 \times 10^3 T_9$	$\times 2$	
(10) $^{12}\text{C}(n, \gamma)^{13}\text{C}$	$4.64 \times 10^2 + 5.71 \times 10^3 T_9$	$\pm 10\%$	Nagai et al. 1991a
(11) $^{13}\text{C}(n, \gamma)^{14}\text{C}$	$1.82 \times 10^2 + 4.633 \times 10^4 T_9^{-3/2} \exp(-1.636/T_9)$	$\times 2$	Raman et al. 1990
(12) $^{14}\text{C}(n, \gamma)^{15}\text{C}$	$7.8 \times 10^2 T_9 + 2.05 \times 10^3 T_9^{-3/2} \exp(-21.14/T_9)$	$\times 4$	Beer et al. 1992
(13) $^{15}\text{C}(n, \gamma)^{16}\text{C}$	$5.27 \times 10^2 T_9 + 3.28 \times 10^4 T_9^{-3/2} \exp(-21.56/T_9)$	$\times 2$	Rauscher et al. 1994
(14) $^{16}\text{C}(n, \gamma)^{17}\text{C}$	$3.66 \times 10^2 T_9$	$\times 2$	Rauscher et al. 1994
(15) $^{17}\text{C}(n, \gamma)^{18}\text{C}$	$1.100 \times 10^3 + 4.05 \times 10^1 T_9 + 1.133 \times 10^3 T_9^{-3/2} \exp(-0.541/T_9)$	$\times 10$	
(16) $^{18}\text{C}(n, \gamma)^{19}\text{C}$	$1.014 \times 10^3 + 3.377 \times 10^2 T_9$	$\times 2$	Nakamura et al. 1999
(17) $^{19}\text{C}(n, \gamma)^{20}\text{C}$	$2.10 \times 10^2 + 1.02 \times 10^1 T_9 + 3.74 \times 10^2 T_9^{-3/2} \exp(-0.75/T_9)$	$\times 10$	
(18) $^{18}\text{C}(\alpha, n)^{21}\text{O}$	$1.659 \times 10^{13} T_9^{-2/3} \exp(-27.5 T_9^{-1/3})$	$\times 10$	

a) $T_{9*} = T_9 / (1.0 + 0.1378 T_9)$,

b) Percentage of 1σ uncertainty. Otherwise, factor two ($\times 2$), four ($\times 4$) and ten ($\times 10$) uncertainties.

c) Blank means the present estimates, as explained in the text.

Table 2:

	Fast Wind Model ^a	Slow Wind Model ^b
s/k	300	385.7
τ_{dyn}	0.005 s	0.300 s ^c
$Y_{e,i}$	0.45	0.3623
T_a	0.60	1.04 ^c

a Otsuki et al. (2003).

b Woosley et al. (1994). These are the asymptotic values from Table 1 of Woosley et al. (1994).

c Woosley et al. (1994). These are the values read off from the trajectory-40.

Table 3: Three exponential-model parameter sets for studying the dependence of the r-process on τ_{dyn} .

τ_{dyn}	0.50	5.0	50
s/k	200	350	1700
Y_e	0.45	0.45	0.45
T_a	0.60	0.60	0.60

Table 4: The same as table 3, but for s/k .

τ_{dyn}	1.0	1.0	1.0
s/k	200	300	400
Y_e	0.20	0.35	0.45
T_a	0.60	0.60	0.60

Table 5: The same as table 3, but for Y_e .

τ_{dyn}	5.0	5.0	5.0
s/k	200	300	350
Y_e	0.20	0.35	0.45
T_a	0.60	0.60	0.60

Table 6: The same as table 3, but for T_a .

τ_{dyn}	5.0	5.0	5.0
s/k	250	350	350
Y_e	0.45	0.45	0.45
T_a	0.52	0.62	0.72

Table 7: Sensitivity result for the 2nd and 3rd r-process peak elements and actinides ^{232}Th , ^{235}U and ^{238}U in the fast flow model. The last two column show $\pm 2\sigma$ current importance of each reaction. See the definition in text.

No.	reaction	sensitivity(α_i)					current	
		2nd peak	3rd peak	^{232}Th	^{235}U	^{238}U	importance($\pm 2\sigma$)	
(1)	$\alpha(\text{an}, \gamma)^9\text{Be}$	0.1823	-0.6546	-1.9423	-1.9819	-2.1006	0.3445	11.2222
(2)	$\alpha(\text{t}, \gamma)^7\text{Li}$	0.2874	-0.7474	-2.7125	-2.7857	-2.9583	0.2658	13.2353
(3)	$^7\text{Li}(\text{n}, \gamma)^8\text{Li}$	0.0465	-0.0917	-0.4296	-0.4436	-0.4729	0.7881	1.7163
(4)	$^8\text{Li}(\alpha, \text{n})^{11}\text{B}$	0.0017	-0.0032	-0.0164	-0.0170	-0.0181	0.9882	1.0120
(5)	$^9\text{Be}(\text{n}, \gamma)^{10}\text{Be}$	0.0042	-0.0105	-0.0337	-0.0346	-0.0365	0.9761	1.0245
(6)	$^{11}\text{B}(\text{n}, \gamma)^{12}\text{B}$	-0.0100	0.0096	0.1119	0.1166	0.1256	1.0853	0.9214
(7)	$^{12}\text{B}(\text{n}, \gamma)^{13}\text{B}$	0.0015	-0.0079	-0.0114	-0.0115	-0.0012	0.9944	1.0056
(8)	$^{13}\text{B}(\text{n}, \gamma)^{14}\text{B}$	0.0	0.0	0.0	0.0	0.0	1.0	1.0
(9)	$^{14}\text{B}(\text{n}, \gamma)^{15}\text{B}$	0.00010	-0.0002	-0.0032	-0.0034	-0.0035	0.9977	1.0024
(10)	$^{12}\text{C}(\text{n}, \gamma)^{13}\text{C}$	0.0	0.0	0.0	0.0	0.0	1.0	1.0
(11)	$^{13}\text{C}(\text{n}, \gamma)^{14}\text{C}$	0.0005	-0.0045	-0.0214	-0.0227	-0.0232	0.9846	1.0157
(12)	$^{14}\text{C}(\text{n}, \gamma)^{15}\text{C}$	0.0	0.0	0.0	0.0	0.0	1.0	1.0
(13)	$^{15}\text{C}(\text{n}, \gamma)^{16}\text{C}$	0.0040	-0.0194	-0.0899	-0.0878	-0.0867	0.9407	1.0630
(14)	$^{16}\text{C}(\text{n}, \gamma)^{17}\text{C}$	0.0	0.0	0.0	0.0	0.0	1.0	1.0
(15)	$^{17}\text{C}(\text{n}, \gamma)^{18}\text{C}$	0.0274	-0.0209	-0.1624	-0.1735	-0.1767	0.6747	1.4821
(16)	$^{18}\text{C}(\text{n}, \gamma)^{19}\text{C}$	0.0	0.0	0.0	0.0	0.0	1.0	1.0
(17)	$^{19}\text{C}(\text{n}, \gamma)^{20}\text{C}$	0.0	0.0	0.0	0.0	0.0	1.0	1.0
(18)	$^{18}\text{C}(\alpha, \text{n})^{21}\text{O}$	0.0233	-0.0017	-0.0285	-0.0288	-0.0298	0.9354	1.0691

Table 8: Sensitivity result for the 2nd r-process peak elements in the slow wind model. The last two column show $\pm 2\sigma$ current importance of each reaction. See the definition in text.

No.	reaction	sensitivity(α_i)	current importance($\pm 2\sigma$)	
(1)	$\alpha(\alpha n, \gamma)^9\text{Be}$	0.2388	1.1351	0.7502
(2)	$\alpha(t, \gamma)^7\text{Li}$	-0.1377	0.9373	1.1345
(3)	$^7\text{Li}(n, \gamma)^8\text{Li}$	-0.0486	0.9745	1.0603
(4)	$^8\text{Li}(\alpha, n)^{11}\text{B}$	-0.0056	0.9961	1.0039
(5)	$^9\text{Be}(n, \gamma)^{10}\text{Be}$	0.0	1.0	1.0
(6)	$^{11}\text{B}(n, \gamma)^{12}\text{B}$	-0.0005	0.9997	1.0003
(7)	$^{12}\text{B}(n, \gamma)^{13}\text{B}$	0.0	1.0	1.0
(8)	$^{13}\text{B}(n, \gamma)^{14}\text{B}$	0.0	1.0	1.0
(9)	$^{14}\text{B}(n, \gamma)^{15}\text{B}$	0.0	1.0	1.0
(10)	$^{12}\text{C}(n, \gamma)^{13}\text{C}$	0.0	1.0	1.0
(11)	$^{13}\text{C}(n, \gamma)^{14}\text{C}$	-0.0016	0.9963	1.0037
(12)	$^{14}\text{C}(n, \gamma)^{15}\text{C}$	0.0	1.0	1.0
(13)	$^{15}\text{C}(n, \gamma)^{16}\text{C}$	0.0	1.0	1.0
(14)	$^{16}\text{C}(n, \gamma)^{17}\text{C}$	0.0	1.0	1.0
(15)	$^{17}\text{C}(n, \gamma)^{18}\text{C}$	0.0	1.0	1.0
(16)	$^{18}\text{C}(n, \gamma)^{19}\text{C}$	0.0	1.0	1.0
(17)	$^{19}\text{C}(n, \gamma)^{20}\text{C}$	0.0	1.0	1.0
(18)	$^{18}\text{C}(\alpha, n)^{21}\text{O}$	0.0	1.0	1.0

Table 9: Sensitivity results for the 2nd and 3rd r-process peak elements and actinides Th, ^{235}U and ^{238}U . The parameters of the fast wind model are $\tau_{dyn}=0.5$ ms, $s/k=200$ and $Y_e=0.45$. The last two column show $\pm 2\sigma$ current importance of each reaction. See the definition in text.

No.	reaction	2nd peak	3rd peak	Th	^{235}U	^{238}U	current importance($\pm 2\sigma$)	
(1)	$\alpha(\alpha n, \gamma)^9\text{Be}$	0.0632	-0.6108	-1.4546	-1.4689	-1.5412	0.4540	6.0002
(2)	$\alpha(t, \gamma)^7\text{Li}$	0.0498	-0.9534	-2.1597	-2.1774	-2.2954	0.3538	7.5819
(3)	$^7\text{Li}(n, \gamma)^8\text{Li}$	-0.0050	0.0197	0.0641	0.0641	0.0657	1.0349	0.9251
(4)	$^8\text{Li}(\alpha, n)^{11}\text{B}$	-0.0004	0.0012	0.0047	0.0048	0.0048	1.0033	0.9967
(5)	$^9\text{Be}(n, \gamma)^{10}\text{Be}$	0.0001	-0.0009	-0.0027	-0.0027	-0.0029	0.9981	1.0019
(6)	$^{11}\text{B}(n, \gamma)^{12}\text{B}$	0.0015	-0.0073	-0.0200	-0.0199	-0.0209	0.9861	1.0141
(15)	$^{17}\text{C}(n, \gamma)^{18}\text{C}$	-0.0032	-0.0169	-0.0402	-0.0405	-0.0442	0.9086	1.1006

Table 10: The same as table 9, but for the parameters of the fast wind model $\tau_{dyn}=5$ ms, $s/k=350$ and $Y_e=0.45$.

No.	reaction	2nd peak	3rd peak	Th	^{235}U	^{238}U	current importance($\pm 2\sigma$)	
(1)	$\alpha(\alpha n, \gamma)^9\text{Be}$	0.0906	-0.2290	-0.7554	-0.7661	-0.8133	0.6617	2.5523
(2)	$\alpha(t, \gamma)^7\text{Li}$	0.6500	-1.2696	-4.9599	-5.0445	-5.3809	0.0898	109.8522
(3)	$^7\text{Li}(n, \gamma)^8\text{Li}$	0.1244	-0.1587	-0.8138	-0.8305	-0.8879	0.6390	2.7628
(4)	$^8\text{Li}(\alpha, n)^{11}\text{B}$	0.0046	-0.0051	-0.0298	-0.0305	-0.0325	0.9788	1.0271
(5)	$^9\text{Be}(n, \gamma)^{10}\text{Be}$	0.0025	-0.0043	-0.0158	-0.0160	-0.0171	0.9888	1.0114
(6)	$^{11}\text{B}(n, \gamma)^{12}\text{B}$	-0.0049	-0.0171	0.0583	0.0599	0.0690	1.0442	0.9577
(15)	$^{17}\text{C}(n, \gamma)^{18}\text{C}$	0.0124	-0.0356	-0.1271	-0.1278	-0.1409	0.7380	1.3550

Table 11: The same as table 9, but for the parameters of the fast wind model $\tau_{dyn}=50$ ms, $s/k=1700$ and $Y_e=0.45$.

No.	reaction	2nd peak	3rd peak	Th	²³⁵ U	²³⁸ U	current importance($\pm 2\sigma$)	
(1)	$\alpha(\alpha n, \gamma)^9\text{Be}$	0.0045	-0.0099	-0.0304	-0.0306	-0.0330	0.9835	1.0384
(2)	$\alpha(t, \gamma)^7\text{Li}$	1.5255	-1.9525	-8.4970	-8.6190	-9.1254	0.0164	3025.7589
(3)	$^7\text{Li}(n, \gamma)^8\text{Li}$	0.5260	-0.5790	-2.8761	-2.9151	-3.0879	0.2079	35.2829
(4)	$^8\text{Li}(\alpha, n)^{11}\text{B}$	0.0552	-0.0613	-0.2939	-0.2985	-0.3155	0.8108	1.2334
(5)	$^9\text{Be}(n, \gamma)^{10}\text{Be}$	0.0005	-0.0012	-0.0029	-0.0028	-0.0031	0.9980	1.0020
(6)	$^{11}\text{B}(n, \gamma)^{12}\text{B}$	0.0009	-0.0294	-0.0295	-0.0295	-0.0282	0.9801	1.0204
(15)	$^{17}\text{C}(n, \gamma)^{18}\text{C}$	0.0779	-0.1152	-0.4049	-0.4111	-0.4347	0.3829	2.6116

Table 12: The same as table 9, but for the parameters of the fast wind model $\tau_{dyn}=5$ ms, $s/k=200$ and $Y_e=0.20$

No.	reaction	2nd peak	3rd peak	Th	²³⁵ U	²³⁸ U	current importance($\pm 2\sigma$)	
(1)	$\alpha(\alpha n, \gamma)^9\text{Be}$	0.0767	-0.1616	-0.2529	-0.2416	-0.2585	0.8753	1.3528
(2)	$\alpha(t, \gamma)^7\text{Li}$	0.8267	-1.2469	-2.5047	-2.5057	-2.4766	0.3094	9.8430
(3)	$^7\text{Li}(n, \gamma)^8\text{Li}$	0.1484	-0.1782	-0.4368	-0.4371	-0.4415	0.7924	1.6954
(4)	$^8\text{Li}(\alpha, n)^{11}\text{B}$	0.0283	-0.0335	-0.0812	-0.0810	-0.0821	0.9451	1.0581
(5)	$^9\text{Be}(n, \gamma)^{10}\text{Be}$	0.0084	-0.0112	-0.0235	-0.0236	-0.0231	0.9839	1.0164
(6)	$^{11}\text{B}(n, \gamma)^{12}\text{B}$	-0.0247	-0.0072	0.1097	0.1115	0.1181	1.0815	0.9246
(15)	$^{17}\text{C}(n, \gamma)^{18}\text{C}$	-0.0025	0.0102	-0.0022	-0.0028	-0.0030	0.9939	1.0062

Table 13: The same as table 9, but for the parameters of the fast wind model $\tau_{dyn}=5$ ms, $s/k=300$ and $Y_e=0.35$.

No.	reaction	2nd peak	3rd peak	Th	^{235}U	^{238}U	current importance($\pm 2\sigma$)	
(1)	$\alpha(\alpha n, \gamma)^9\text{Be}$	0.0879	-0.1810	-0.5383	-0.5502	-0.5724	0.7454	1.9475
(2)	$\alpha(t, \gamma)^7\text{Li}$	0.7862	-1.2755	-4.4828	-4.5748	-4.8373	0.1134	69.6807
(3)	$^7\text{Li}(n, \gamma)^8\text{Li}$	0.1466	-0.1774	-0.7737	-0.7914	-0.8407	0.6534	2.6261
(4)	$^8\text{Li}(\alpha, n)^{11}\text{B}$	0.0118	-0.0102	-0.0552	-0.0580	-0.0577	0.9613	1.0403
(5)	$^9\text{Be}(n, \gamma)^{10}\text{Be}$	0.0059	-0.0097	-0.0318	-0.0320	-0.0349	0.9775	1.0231
(6)	$^{11}\text{B}(n, \gamma)^{12}\text{B}$	-0.0222	-0.0078	0.1662	0.1714	0.1887	1.1293	0.8855
(15)	$^{17}\text{C}(n, \gamma)^{18}\text{C}$	0.0021	0.0021	-0.0268	-0.0275	-0.0307	0.9368	1.0674

Table 14: β -decay lifetimes in units of s, and the neutron separation energies (S_n) in units of MeV. The S_n -value for ^{19}C was changed from 0.191 MeV to 0.530 MeV (Nakamura et al. 1999).

	^{15}C	^{16}C	^{17}C	^{18}C	^{19}C	^{20}C
β -life time[s]	2.449	0.747	0.193	0.092	0.049	0.014
S_n [MeV]	4.250	0.725	4.191	0.191	→0.530	3.345